Time-dependent regulation of cytokine production by RNA binding proteins defines T cell effector function

Branka Popović[1], Aurélie Guislain[1], Sander Engels[1], Benoît P. Nicolet[1], Anouk P. Jurgens[1], Natali Paravinja[1], Julian J. Freen-van Heeren[1], Floris P.J. van Alphen[2], Maartje van den Biggelaar[2], Fiamma Salerno[1,3], and Monika C. Wolkers[1*]

[1]Department of Hematopoiesis, Sanquin Research-Amsterdam UMC Landsteiner Laboratory and Oncode Institute, Utrecht, The Netherlands

[2]Department of Molecular Hematology, Sanquin Research, Amsterdam, The Netherlands

[3]Present address: Immunology programme, The Babraham Institute, Cambridge, UK

*Corresponding author: M. Wolkers, Sanquin Research, Department of Hematopoiesis, Plesmanlaan 125, 1066 CX Amsterdam, The Netherlands. Tel: +31-6-24268490; Fax: +31-20-5123474; Email: m.wolkers@sanquin.nl

Summary

Effective T cell responses against target cells require controlled production of the key pro-inflammatory cytokines IFN-γ, TNF and IL-2. Post-transcriptional events determine the magnitude and duration of cytokine production in T cells, a process that is largely regulated by RNA binding proteins (RBPs). Here we studied the identity and mode of action of RBPs interacting with cytokine mRNAs. With an RNA aptamer-based capture assay from human T cell lysates, we identified >130 RBPs interacting with the full length 3'untranslated regions of *IFNG*, *TNF* and *IL2.* The RBP landscape altered upon T cell activation. Furthermore, RBPs display temporal activity profiles to control cytokine production. Whereas HuR promotes early cytokine production, the peak production levels and response duration is controlled by ZFP36L1, ATXN2L and ZC3HAV1. Importantly, ZFP36L1 deletion boosts T cell responses against tumors *in vivo,* revealing the potential of the RBP map to identify critical modulators of T cell responses.

Keywords

T cells, cytokines, post-transcritpional regulation, RNA-binding proteins, ZFP36L1, HuR, ATXN2L, ZC3HAV1, tumor-infiltrating T cells

Introduction

T cells are critical players to fight infections and to clear malignant cells. To do so, they produce effector molecules such as granzymes and proinflammatory cytokines. Interferon gamma (IFN-γ) and Tumor necrosis factor (TNF) are major contributors to the anti-microbial and anti-tumoral effects of T cells (Zhang *et al.*, 2008; Patel *et al.*, 2017). Furthermore, T cells that co-produce IFN-γ and TNF together with the proliferation and survival-inducing cytokine IL-2 are considered the most potent anti-viral and anti-tumoral $CD8^+$ and $CD4^+$ T cells in humans (Almeida *et al.*, 2007; Ciuffreda *et al.*, 2008; Quezada *et al.*, 2010; Wimmers *et al.*, 2016; Oh *et al.*, 2020).

Whereas the mode of action of cytokines on target cells is well established, much less is known about the molecular switches that drive their production. Recent studies revealed that post-transcriptional regulation (PTR) is essential in determining the magnitude and duration of cytokine production (Yoshinaga *et al.*, 2019; Salerno *et al.*, 2020; Jurgens *et al.*, 2021). PTR defines RNA splicing and RNA modifications, the nuclear export and further subcellular localization, mRNA stability and translation efficiency. These post-transcriptional events are controlled by signals that T cells receive. We previously showed that the TCR signal strength together with costimulatory signals define the mRNA synthesis and degradation rate and regulate translation and translation efficiency of cytokines in T cells (Salerno *et al.*, 2016, 2017, 2019).

The importance of PTR in immune cell function was revealed when AU-rich sequences (AREs) were deleted from the germ-line *Tnf* and *Ifng* 3'Untranslated region (3'UTR) in mice. This resulted in hyperinflammation and immunopathology due to aberrant cytokine production (Kontoyiannis *et al.*, 1999; Hodge *et al.*, 2014). Conversely, tumor-infiltrating T cells (TILs) fail to produce IFN-γ despite their continuous expression of *Ifng* mRNA, which points to post-transcriptional dysregulation of cytokine production within tumors (Salerno *et al.*, 2019). Indeed, removing AREs from the *Ifng* 3'UTR restored the IFN-γ protein production in murine TILs, and it augmented and prolonged protein production in human T cells (Salerno *et al.*, 2019; Freen-van Heeren *et al.*, 2020). These studies thus underpin the critical role of 3'UTRs as key regulators for cytokine production in T cells.

RNA binding proteins (RBPs) are critical mediators of PTR (Akira *et al.*, 2021). For instance, the RBPs ZC3H12A (Regnase-1) and Roquin-1 prevent naïve $CD4^+$ T cells from exiting their quiescent state. By interacting with the 3'UTR, they destabilize mRNAs that encode key regulators of $CD4^+$ T cell differentiation and function (Hoefig *et al.*, 2018). In contrast, Arid5a modulates T cell differentiation by stabilizing *Stat3* and *Ox40* mRNA upon T cell activation (Masuda *et al.*, 2016; Hanieh *et al.*, 2018). We recently showed that the ARE-binding protein ZFP36L2 blocks translation of pre-formed cytokine mRNAs in memory T cells, which prevents aberrant protein production from these ready-to-deploy mRNAs in the absence of TCR stimuli (Salerno *et al.*, 2018). Importantly, re-activating memory T cells released pre-formed *Tnf* and *Ifng* mRNA from ZFP36L2, allowing for immediate cytokine production (Salerno *et al.*, 2018). Thus, RBP binding to target mRNAs can rapidly change, which in turn can have a major impact on the acquisition and execution of T cell effector function. A comprehensive study on RBP interactions to target mRNAs in T cells is however lacking.

To decipher RNA targets of specific RBPs, Cross-linked immunoprecipitation (CLIP) methods have been developed (König *et al.*, 2010), and our understanding of RBP-mRNA interactions substantially advanced with the recently generated 150 RBP interaction maps (Van Nostrand *et al.*, 2020). However, these studies performed in epithelial cell lines are not directly translatable to T cells. Not only different target mRNAs are expressed in T cells, but also RBP expression is cell-type specific and alters during T cell differentiation and activation (Salerno *et al.*, 2020; Jurgens *et al.*, 2021; Zandhuis *et al.*, 2021). More than 2000 RBPs have been identified (Gerstberger *et al.*, 2014; Castello *et al.*, 2016; Perez-Perri *et al.*, 2018). Which of these RBPs interact with cytokine mRNA, and how RNA binding alters upon T cell activation is to date unexplored. To answer this question, an RNA-centric approach is required.

Here, we provide the first comprehensive analysis of RBP-mediated regulation of T cell effector function. With an unbiased RNA aptamer pull-down from primary human T cell lysates with the full-length 3'UTRs of IFN-γ, TNF and IL-2, we identified >130 RBPs that interact with cytokine 3'UTRs. RNA-RBP interactions depended on the T cell activation status, and RBPs employed RBP-specific post-transcriptional

mechanisms to control cytokine production. Importantly, genetic deletion of the RBP ZFP36L1, which dampened cytokine production in activated T cells, resulted in improved anti-tumoral T cell responses *in vivo,* revealing the critical role of RBPs in defining T cell effector function.

Results

Cytokine 3'UTRs define protein production in murine and human T cells

To determine how cytokine 3'UTRs contribute to protein production, we retrovirally transduced OT-I T cell receptor (TCR) transgenic $CD8^+$ T cells with reporter constructs containing the full length 3'UTR of the murine *Gzmb, Ifng, Tnf* or *Il2* mRNA fused to the coding sequence of GFP (Figure 1A). The empty GFP construct was used as control ($GFP_{control}$). After 4 days of culture, we measured the GFP geometric mean fluorescence intensity (gMFI). In resting cells, the *Ifng*, *Tnf* and *Il2* 3'UTRs substantially reduced the GFP protein expression levels compared to $GFP_{control}$, or to GFP-Gzmb-3'UTR (Figure 1A, Figure S1A). *Gzmb* 3'UTR also lowered GFP expression levels compared to $GFP_{control}$, but much less so than cytokine 3'UTRs. Activating T cells with $OVA_{257–264}$ peptide showed limited to no alterations in protein expression for $GFP_{control}$ and GFP-Gzmb-3'UTR. In sharp contrast, the GFP protein expression significantly increased for GFP-Ifng-3′UTR, GFP-Tnf-3′UTR and GFP-Il2-3'UTR at 6 h, and even more so at 16 h of activation (Figure 1A). Similar results were obtained with the full length 3'UTRs of human *IFNG*, *TNF* and *IL2:* the GFP protein expression was blocked in resting $CD8^+$ and $CD4^+$ peripheral blood-derived human T cells, and T cell activation with PMA/Ionomycin or α-CD3/α-CD28 boosted the protein expression (Figures 1B, Figure S1). This profound regulation of protein expression by the 3'UTRs of *IFNG, TNF,* and *IL2* is thus conserved between mouse and human.

Identification of RBPs interacting with full length cytokine 3'UTRs

RNA binding proteins (RBPs) are critical modulators of mRNA fate and metabolism, yet their binding to cytokine 3'UTRs in T cells remains ill defined. To identify RBPs that specifically interact with cytokine 3'UTRs, we generated *in vitro* transcribed streptavidin-binding 4xS1m RNA aptamers (Leppek *et al.*, 2014) fused to the full length 3'UTRs of *IFNG*, *TNF,* and *IL2*. An empty 4xS1m RNA aptamer was used as control (Figure 2A). Because RBPs are expressed in a cell-type specific manner (Zandhuis *et al.*, 2021), we used human T cell lysates (Figure 2A). Upon capture of RNA-RBP complexes with streptavidin beads, RNA-interacting proteins were identified by mass spectrometry (MS). Pull-down methods enrich for specific interactors, which results in different protein concentrations and data distribution between pull-down samples and controls (Figure S2A, B). Therefore, we analysed protein raw intensities to identify putative binders. We detected in total 1808 proteins

in all replicates of at least one condition in one independent experiment (Figure S2A, Table S1). Due to the non-normal data distribution in one of the triplicates of *IFNG* 3'UTR, we excluded this sample from the analysis (Figure S2B). Of the 1808 detected proteins, 598 proteins detected in at least 2 of the 3 replicates were enriched with $\log_2$ fold change (LFC)>4 (>16-fold) in cytokine 3'UTR aptamer pull-downs compared to empty aptamer control. Of these, 307 proteins (51.3%) were experimentally confirmed or computationally predicted RBPs (n=222 and n=85, respectively; see Methods). In the downstream analysis, we only included RBPs that were enriched in at least two independently performed experiments. This resulted in 93 RBPs that were identified with the *IFNG* 3′ UTR, 69 RBPs with the *TNF* 3′ UTR, and 82 RBPs with the *IL2* 3′ UTR
(Figure 2B and 2D, and Table S1). When we performed Gene ontology (GO) analysis on all 138 detected RBPs, we found that the terms RNA processing and (m)RNA metabolic processes were enriched (Figure 2C). Translation was in particular enriched in *IFNG*- and *TNF*-associated RBPs, and RNA splicing in *IFNG* and *IL2*-associated RBPs (Figure 2C, Table S2).

Interestingly, some RBPs were identified with more than one cytokine 3'UTR. For instance, NOLC1 and CHERP interacted with the *IFNG* and *TNF* 3'UTRs (Figure 2D, Table S1). The splicing factor SYNCRIP was detected with the *IFNG* and *IL2* 3'UTRs, and nuclear mRNA export protein ZC3H11A and HNRNPAB with *TNF* and *IL2* 3'UTRs (Figure 2D, Table S1). RBPs interacting with all three cytokine 3'UTRs included components of the cleavage and polyadenylation specificity factor complex CPSF1, CPSF2, CPSF4 and FIP1L1 and the ARE-binding proteins ZFP36L1 and HuR (ELAVL1) (Figure 2D, Table S1). ZFP36L2, which we previously identified to bind to preformed *Ifng* and *Tnf* mRNA in memory T cells (Salerno *et al.*, 2018), was also detected, but with LFCs of 2.5 (*IFNG)*, 1.9 (*TNF)* and 3.3 (*IL2),* and did not meet our stringent cut off of LFC>4 (Table S1). Other RBPs were enriched for only one cytokine 3'UTR, such as FMR1 autosomal homolog 2, FXR2, zinc-finger protein ZC3HAV1 and RBM27 for the *IFNG* 3'UTR, stress granule-components ATXN2 and ATXN2L and poly(A)-tail-binding proteins PABPC1 for the *IL2* 3'UTR, and Pumilio homolog 1, PUM1, and RBM15 for the *TNF* 3'UTR (Figure 2D, Table S1). In conclusion, we here identified 138 RBPs in primary human T cells interacting with one or more full length cytokine 3'UTRs.

The RBP binding landscape alters upon T cell activation

T cell activation drives cytokine production, and post-transcriptional events are critical to tightly control the production of these perilous molecules. External triggers can alter the expression and/or post-translational modifications of RBPs, which in turn can alter their RNA binding capacity (Coelho *et al.*, 2017; Grammatikakis *et al.*, 2017; Salerno *et al.*, 2018). To determine how T cell activation modulated the RBP binding landscape to cytokine 3'UTRs, we not only performed the aptamer pull-down with cytosolic lysates from resting T cells, but also from paired samples of T cells activated with PMA/Ionomycin for 2 h (Figure 3A). We detected in total 1596 proteins in all replicates of at least one pulldown condition (Figure S2C, Table S3). Of these 1596 proteins, 443 proteins were enriched with a LFC>4 in cytokine 3'UTR samples compared to empty 4xS1m aptamer control. 244 proteins were annotated as RBPs, of which 77 were detected in two independently performed experiments (Figure 3A, Table S3). 58 of these 77 RBPs displayed enriched binding with an LFC>4 to *IFNG* 3′UTR, 63 RBPs to *TNF* 3′UTR, and 22 RBPs to the *IL2* 3′UTR (Figure 3A). We then studied GO terms of the intified RBPs. IL2 was left with only 3 RBPs that were reproducibly identified in both experiments with an LFC>4, and was therefore excluded from this analysis. RBPs interacting with *IFNG* and *TNF* 3'UTRs 3'UTRs in activated T cells were enriched for GO terms related to RNA processing and (m)RNA metabolic processes (Figure 3B, Table S4).

We next determined whether RBPs alter their RNA binding profile upon T cell activation. Interestingly, the interaction of the ARE-binding protein ZFP36L1 to all three cytokine 3'UTRs considerably increased after T cell activation (Figure 3A and 3C). Other RBPs with enriched binding included m6A-methylation reader YTH domain-containing family protein 1 (YTHDF1) to *IFNG* 3'UTR, and ribosomal RNA processing protein 1 homolog B (RRP1B) to *TNF* 3'UTR. RBPs enriched for the *IL2* 3′UTR included RRM-containing protein (RBM42), PC4 and SFRS1-interacting protein (PSIP1) and WARS (Figure 3C). In contrast, T cell activation resulted in undetectable RNA binding by ZC3H12D (Regnase-4) and uridylyltransferase ZCCHC11 to all three cytokine 3'UTRs, PABPN1 to *IFNG* 3'UTR, ATP-dependent RNA helicase DDX39A and ZNHIT6 to *TNF* 3'UTR*,* and DDX46 and USO1 to *IL2* 3'UTR (Figure 3C).

To define whether the alterations of RBP binding to cytokine 3'UTRs resulted from altered RBP expression levels, we compared the RBP protein expression of the total cytosolic cell lysates from activated and non-activated T cells by MS analysis (Figure 3D, Table S5). Of the RBPs that showed increased interaction with cytokine 3'UTRs upon T cell activation, only ZFP36L1 also showed increased protein expression (Figure 3D, Figure S2D). WARS and YTHDF1 increased their binding to cytokine 3'UTRs upon T cell activation, even though their protein expression was unaltered (Figure 3D, Figure S2D). Conversely, the decreased interaction of ZC3H12D with cytokine 3'UTRs upon T cell activation coincided with decreased protein expression, yet DDX39A and DDX46 lost their interaction to cytokine 3'UTRs without altering their expression levels (Figure 3D, Figure S2D). In conclusion, T cell activation results in dynamic changes of the RBP binding landscape to cytokine 3'UTRs, which can only partially be explained by altered RBP protein expression.

ZFP36L1 regulates cytokine production in T cells in a time-dependent manner

We next questioned which of the RBPs interacting with cytokine 3'UTRs modulated the cytokine production. We turned our attention to ZFP36L1 (TIS11B), one of the top candidates that displayed increased interaction with cytokine 3'UTRs upon T cell activation (Figure 2D, 3C). ZFP36L1 is an ARE-binding zinc-finger RBP that promotes mRNA degradation and represses translation (Lykke-Andersen *et al.*, 2005; Bell *et al.*, 2006; Moore *et al.*, 2018). Together with ZFP36L2, ZFP36L1 limits cell cycle progression in thymocytes and enables T cell maturation (Hodson *et al.*, 2010; Vogel *et al.*, 2016).

We first confirmed ZFP36L1 binding to endogenous *IFNG*, *TNF* and *IL2* mRNA using native RNA immunoprecipitation (RIP) with cytosolic lysates from human PMA-ionomycin activated T cells (Figure 4A). We then generated ZFP36L1-deficient primary human T cells by CRISPR/Cas9 gene-editing to determine whether ZFP36L1 was functionally relevant (Table S6, Figure 4B). Non-targeting crRNA was used as control. ZFP36L1-knockout (KO) in resting T cells did not result in aberrant cytokine production (Figure S3A). However, ZFP36L1 KO $CD8^+$ T cells reactivated for 4 h with α-CD3/α-CD28 produced more cytokines, as defined by higher percentages of IFN-γ,

TNF, and IL-2-producing T cells, and by higher cytokine production (gMFI levels) per cell when compared to control T cells (Figure 4B, Figure S3B).

We and others previously showed that IFN-γ, TNF, and IL-2 follow individual production kinetics (Han *et al.*, 2012; Nicolet *et al.*, 2017; Salerno *et al.*, 2017). To investigate whether ZFP36L1 modulates the cytokine production kinetics, we reactivated T cells with α-CD3/α-CD28 for 1 h to up to 8 h, and measured temporal snapshots of protein secretion by adding brefeldin A for the last 2 h of activation (Salerno *et al.*, 2017). This assay revealed that ZFP36L1 deletion did not alter the early production kinetics of IFN-γ, TNF, and IL-2 in $CD8^+$ T cells (Figure 4C-D, Figure S3C). Consistent with its protein expression profile in activated T cells (Figure S3D), ZFP36L1 deletion showed the greatest effects on cytokine production between 4-8 h of activation, a feature that was partially conserved in $CD4^+$ T cells (Figure 4C-D, Figure S3E). Zooming in on 8h of activation when the effects of ZFP36L1 deletion were most prominent, compiled data from 6 donors revealed significant increases in percentages and in magnitude of the protein production for all 3 cytokines (gMFI levels) (Figure 4E). Interestingly, whereas IFN-γ and IL-2 displayed the largest differences in percentages of cytokine-producing T cells in ZFP36L1 KO T cells, the TNF production was primarily altered in magnitude, as determined by the gMFI (Figure 4D, E). Thus, ZFP36L1 modulates the cytokine production of human T cells, and does so in a time- and cytokine-dependent manner.

ZFP36L1 destabilizes cytokine mRNA in T cells

To investigate whether ZFP36L1 affects the stability of cytokine mRNAs, we activated human T cells with for 3h α-CD3/α-CD28 and then treated them with Actinomycin D (ActD) to block *de novo* transcription. qRT-PCR analysis revealed that the half-life of *IFNG* and *IL2* mRNA was between 50-60 min in control T cells, and that of *TNF* mRNA between 20-30 min (Figure 4F). ZFP36L1 deletion substantially increased the half-life of all three cytokine mRNAs to >120 min for *IFNG* and *IL2*, and to 40-50 min for *TNF* mRNA (Figure 4F). The increased mRNA stability also resulted in higher overall cytokine mRNA expression levels in activated ZFP36L1 KO T cells compared to control T cells (Figure 4G). Intriguingly, a co-immunoprecipitation assay with α-ZFP36L1 from activated human T cell lysates identified several components of

the mRNA degradation machinery, including members of the CCR4-NOT complex, i.e. CNOT3, CNOT4, CNOT6L, CNOT7, CNOT10, CNOT11, and of the RNA 3'->5' exosome complex, i.e. EXOSC1, EXOSC2, EXOSC5, EXOSC6, EXOSC7, EXOSC8, EXOSC9 (Figure 4H, Figure S3F). These proteins were only detected upon immunoprecipitation with α-ZFP36L1, but not with the IgG control. Thus, ZFP36L1 dampens cytokine production in T cells by destabilizing their mRNA.

RBPs differentially modulate cytokine production in T cells

We next investigated other RBPs that were identified with the pull-down assay. We followed up on FXR2, ZC3HAV1, ATXN2L and HuR, four RBPs that showed strong binding to the cytokine 3'UTRs in resting, and in activated T cells (Figure 2D). CRISPR/Cas9 gene-editing in human T cells substantially reduced the protein expression of all four RBPs (Figure 5A). Deleting FXR2 in α-CD3/α-CD28 activated T cells had no effect on cytokine expression when compared to the donor-matched control (Figure 5A, Figure S4A). ATXN2L and ZC3HAV1 deletion, however, resulted in higher percentages of IFN-γ, TNF and IL-2 producing $CD8^+$ T cells at 4 h after activation (Figure 5A, Figure S4A). In contast, reduced protein expression of HuR diminished the cytokine production in $CD8^+$ T cells (Figure 5A, Figure S4A). In line with their measured effect on cytokine production, ATXN2L, ZC3HAV1 and HuR directly interacted with endogenous cytokine mRNA, as determined by native RIP (Figure 5B). Interestingly, the preference for specific cytokine RNAs observed in the aptamer pull-down assay (Figure 2D) was also reflected by the native RIP: the ATXN2L RIP showed highest enrichment for *IL2* mRNA, and the HuR RIP for *TNF* mRNA (Figure 5B).

To determine at which time points the RBPs ZC3HAV1, ATXN2L and HuR exert their effects on cytokine production, we again performed the snapshot analysis (Figure 5C). Intriguingly, this analysis revealed different kinetics in RBP activity. Similar to the ZFP36L1 KO T cells (Figure 4C), ATXN2L KO increased the cytokine production in activated $CD8^+$ and $CD4^+$ T cells from 4 h onwards, both in terms of percentage and production per cell (Figure 5C and 5D, Figure S4B). ZC3HAV1 deletion also increased the cytokine production from 4 h of activation onwards, yet increases of TNF and IL-2 production per cell were already observed at 1-2 h post T cell activation

(Figure 5C and 5D, Figure S4B). Conversely, HuR deletion decreased the cytokine expression in particular between 1-4 h after T cell activation, and did so most effectively in $CD8^+$ T cells (Figure 5C and 5D, Figure S4B, C).

Intriguingly, whereas ZFP36L1 deletion resulted in stabilized cytokine mRNA, this effect on RNA stability was not observed when ATXN2L, ZC3HAV1, or HuR were deleted (Figure S5A). Also the overall expression of cytokine mRNAs in ATXN2L KO, ZC3HAV1 KO and HuR KO T cells was comparable with the control cells (Figure S5B). In conclusion, CRISPR/Cas9 gene-editing of primary human T cells confirmed the regulatory activity on cytokine production for 4 out of 5 tested RBPs identified in the RBP pull-down assay. These 4 RBPs differentially modulate cytokine production, and at different time points: whereas ATXN2L, ZC3HAV1, and ZFP36L1 dampen the production of IFN-γ, TNF and IL-2 at later stages of T cell activation, HuR boosts the early cytokine production.

RBPs define the cytokine production of T cells in response to antigen-expressing target cells

We next determined how RBP depletion modulated T cell responses to target cells. To test this, we retrovirally transduced T cells with the MART1-specific TCR recognizing the HLA-A*0201-restricted $MART1_{26-35}$ epitope (Gomez-Eerland *et al.*, 2014). Subsequent CRISPR/Cas9 gene editing resulted in efficient RBP deletion (Figure S6A). To study the cytokine production in response to antigen-expressing target cells, we exposed RBP-deficient, and control MART1 TCR expressing T cells to a $MART1^{hi}$ HLA-A*0201^+ melanoma cell line ($MART1^+$), or to a $MART1^{lo}$ HLA-A*0201^- melanoma control cell line ($MART1^-$) (Figure S6B) (Nicolet *et al.*, 2020). ZFP36L1 KO $CD8^+$ T cells were superior cytokine producers compared to control T cells, as revealed by substantially higher IFN-γ, TNF and IL-2 production after 6 h of co-culture (Figure 6A, B). Of the other two tested RBPs, only ZC3HAV1 KO T cells displayed slight, but significant increases in IFN-γ producing cells (Figure 6A, B). In line with their reduced production kinetics at later time points (Han *et al.*, 2012; Nicolet *et al.*, 2017), all T cells showed reduced cytokine production after 24 h of co-culture, in particular of IL-2 and TNF. However, ZFP36L1 KO T cells were able to maintain their IFN-γ and TNF production at this late time point (Figure 6B). This was also evidenced by the polyfunctional cytokine production profile. Whereas only slight

increases of T cells producing 2 or 3 cytokines were found at 6 h of co-culture in ZFP36L1 KO and ZC3HAV1 KO T cells, at 24 h of co-culture, ZFP36L1 KO T cells, and to a lesser extent ATXN2L KO T cells clearly maintained their capacity to (co)-produce IFN-γ and TNF compared to control T cells (Figure 6C).

To determine if different antigen levels are relevant for cytokine production by RBP deficient T cells, we loaded the HLA-A*0201^{+} MART1-negative uveal melanoma cell line 2A14 with increasing amounts of MART1$_{26-35}$ peptide, and we measured the cytokine production after 6h of co-culture with MART1 TCR-expressing T cells. Whereas ZC3HAV1 KO and ATXN2L KO T cells only significantly increased their cytokine production compared to control T cells at high antigen load (100nM), ZFP36L1 KO T cells were superior in producing all three cytokines even at low antigen levels (0.1nM), and this effect was maintained at intermediate and high antigen levels (1 and 100nM, respectively; Figure 6D, 6E, S6C). Thus, the activity of individual RBPs requires different signal strength to exert their modulatory function.

ZFP36L1-deficient anti-tumoral T cells produce more cytokines and delay the tumor outgrowth

Our data reveal that RBP depletion can boost cytokine production in response to target cells. Gradual loss of effector function, and in particular of IFN-γ and TNF is a major hurdle of effective T cell responses (van der Leun *et al.*, 2020; Philip *et al.*, 2021). RBPs are well conserved in mammals (Gerstberger *et al.*, 2014). Therefore, to study whether RBP deletion rescues cytokine production of tumor infiltrating lymphocytes (TILs) *in vivo*, we turned to the murine B16F10 melanoma model. We focused our attention on ZFP36L1, which showed the most potent effects in human T cells. We generated Zfp36l1-deficient OT-I TCR transgenic murine T cells by CRISPR/Cas9 gene-editing (Figure S7A, Table S6), and injected 1x10^{6} Zfp36l1 KO, or control OT-I T cells into tumor-bearing mice that had received 7 days earlier B16-OVA tumor cells expressing Ovalbumin (B16-OVA; Figure 7A) (de Witte *et al.*, 2006). At 14 days post T cell transfer, we analysed the capacity of splenic and tumor-infiltrating OT-I T cells to produce cytokines. In line with our previous findings (Salerno *et al.*, 2019), we only detected cytokine production in splenic OT-I T cells when reactivated with OVA$_{257-264}$ peptide (Figure S7C). We found a slight, but not

significant increase in the percentage of IFN-γ and IL-2 producing Zfp36l1 KO splenic T cells compared to control T cells (Figure S7C).

When we analysed the tumor-infiltrating T cells, we found that the absolute numbers of Zfp36l1 KO and control OT-I TILs did not substantially differ (Figure 7B). To measure the capacity to produce cytokines within the tumor digest, we first incubated the tumor digest *ex vivo* for 2 h with brefeldin A and monensin, without the addition of exogenous peptide. The production of TNF and IL-2 in control OT-I TILs was undetectable, and of IFN-γ very limited, as previously reported (Figure 7C and S7B; (Salerno *et al.*, 2019)). Treatment with exogenous $OVA_{257-264}$ peptide for 4 h only marginally increased the cytokine expression in control OT-I TILs, in particular when compared to reactivated splenic OT-I T cells (Figure 7C, S7B and S7C). Zfp36l1 KO OT-I TILs, however, produced all three cytokines, a feature that was apparent in the presence and absence of exogenous antigen, and for the percentages of cytokine producing TILs as well as for the cytokine production per cell (Figure 7C, S7B and S7C). Thus, the inhibitory role on cytokine production by ZFP36L1 in T cells is conserved between mouse and man. Intriguingly, also other effector molecules such as the degranulation marker CD107a and the cytotoxic molecule Granzyme B were increased in Zfp36l1 KO TILs when compared to control TILs (Figure 7D). This feature appeared to be unique to the tumor environment, because no differences in CD107a and Granzyme B expression were observed in spleen-derived T cells (Figure S7D).

Because both cytokine production and granzyme B expression was higher in Zfp36l1 KO TILs, we questioned if Zfp36l1 deficiency also influenced the tumor outgrowth. We therefore injected a low number ($0.65x10^6$ cells) of Zfp36l1 KO or control OT-I T cells into B16-OVA tumor-bearing mice and followed the tumor growth. Remarkably, even with these low numbers of transferred T cells, the tumor outgrowth of this aggressive tumor was delayed in mice that had received Zfp36l1 KO T cells (Figure 7E). In fact, at 14 days post T cell transfer, i.e. the time point when we measured superior cytokine production and degranulation in Zfp36l1 KO TILs *ex vivo* (Figure 7C and 7D), 3/8 of the control mice and none of the Zfp36l1 KO mice reached the human endpoint of $1000mm^3$ of tumor size (Figure 7F). In conclusion, Zfp36l1 gene-editing in T cells enhances the therapeutic potency of T cell therapy.

Discussion

The fine-tuning of cytokine production by post-transcriptional events is key for appropriate T cell effector function. However, little is known about the mediators responsible for modulating cytokine production. Here, we provide the first RBP catalogue of >130 RBPs that interact with the full length 3'UTRs of IFN-γ, TNF and IL-2 in human T cells.

Notably, RBP interactions with the cytokine 3'UTRs can alter upon T cell activation, as observed for increased binding by ZFP36L1, YTHDF1, WARS and decreased RNA binding by ZC3H12D and DDX39A. In some cases, alterations in RNA binding coincides with altered RBP protein expression (i.e. ZFP36L1, ZC3H12D). However, this is not observed for all RBPs. For example, YTHDF1, WARS and DDX39A change their binding potential upon T cell activation while maintaining their overall protein expression levels. This finding points to other regulatory mechanisms. For instance, RBPs can undergo post-translational modifications, as exemplified by stress-induced HuR phosphorylation that resulted in reduced target mRNA binding in HeLa cells (Kim *et al.*, 2008; Yoon *et al.*, 2014). RBPs can also compete with each other for target binding. For instance, Arid5a and ZC3H12A interact with the same stem loop in the 3'UTR of *STAT3* mRNA in HEK293T cells (Masuda *et al.*, 2016). Similarly, HuR and ZFP36 (Tristetraprolin, TTP) compete for binding to *TNF* and *GM-CSF* mRNA in macrophages and HeLa cells, respectively (Raghavan *et al.*, 2001; Tiedje *et al.*, 2012). Lastly, competition of RBPs with other RNA regulatory molecules such as miRNAs is conceivable (Srikantan *et al.*, 2012). Understanding the mechanisms that define RBP expression and function will be thus critical to further decipher their role in modulating T cell responses.

In this study, we tested 5 identified RBPs, of which 4 modulate the cytokine production in human T cells. Intriguingly, these 4 RBPs display different effects on cytokine production and with different activity kinetics. HuR promotes the cytokine production in human T cells, and does so most prominently at the onset (1-2 h) of T cell activation. This early boost in cytokine production may in particular be relevant for antigen-experienced T cells. These cells contain pre-formed mRNA, and immediate cytokine production is licensed by releasing the ready-to deploy mRNA

from ZFP36L2 (Salerno *et al.*, 2017, 2018). Our data here suggest that this early cytokine production is further facilitated by HuR. The mode of action of HuR is yet to be defined. Because we found no effects on mRNA stability, HuR may rather influence translation efficiency directly, or indirectly by rendering the mRNA accessible to the translation machinery through altering its subcellular localization, or through competing with other RBPs.

In contrast to HuR, the RBPs ZFP36L1, ATXN2L and ZC3HAV1 block cytokine production, and they do so most effectively at the peak (4-8 h), and ZFP36L1 (and ATXN2L) also at prolonged (24 h) T cell activation. ATXN2L and ZC3HAV1 do not affect RNA stability, and thus employ other post-transcriptional events to dampen cytokine production. In epithelial cell lines, ATXN2L regulates stress granules and processing bodies (Kaehler *et al.*, 2012). ZC3HAV1 was shown to destabilize *IFNB and IFNL3* mRNAs in hepatocytes, and human cytomegalovirus RNA in fibroblasts, and it inhibits programmed ribosomal frameshifting of the SARS-CoV-2 virus (Schwerk *et al.*, 2019; Gonzalez-Perez *et al.*, 2021; Zimmer *et al.*, 2021). The mechanisms that ATXN2L and ZC3HAV1 employ in T cells to supress cytokine production, however, await further elucidation.

ZFP36L1 destabilizes all 3 cytokines, and it interacts with regulators of mRNA degradation in activated T cells. One component of the CCR4-NOT complex, CNOT7, was previously shown to interact with ZFP36L1 in 293T cells (Adachi *et al.*, 2014), and is critical for degradation of ZFP36 targets in HeLa cells (Marchese *et al.*, 2010; Sandler *et al.*, 2011). We here identified CNOT7 and several other CNOT proteins together with several exonucleases that possibly contribute to the degradation of target mRNAs of ZFP36L1 in primary T cells. Irrespective of the mode of action, the time point of activity of ZFP36L1, ATXN2L, and ZC3HAV1 clearly indicates their critical contribution in preventing excessive production of cytokines in activated T cells. Having multiple RBP regulators with different modes of action also highlights the need for fine-tuning the cytokine production for appropriate T cell function.

T cells lose their capacity to produce cytokines in the tumor environment. We previously showed that post-transcriptional events substantially contribute to the loss

of IFN-γ production (Salerno *et al.,* 2019; Freen-van Heeren *et al.*, 2020). Here, we report that deleting cytokine-impeding RBPs increases the cytokine production of human T cells when exposed to tumor cells*.* Importantly, the deletion of ZFP36L1 does not only delay the shutdown of cytokine production, but also boosts the effector function of TILs *in vivo*, which leads to better anti-tumoral responses. Deletion of ZFP36L1 does not only improve the production of IFN-γ, but also that of TNF and IL-2, and of the cytotoxic mediators Granzyme B and CD107a, indicating that ZFP36L1 instructs several T cell effector programs. Therefore, ZFP36L1 represents an attractive target to boost anti-tumoral T cell effector responses.

In conclusion, we here provide the first catalogue of dynamic RBP interactions to cytokine mRNAs in human T cells. Our results reveal that this map can serve as a valuable resource for studying the role of RBPs in regulating T cell responses, which can be tested *in vivo* against tumors to identify RBPs as potential targets for therapeutic purposes. Considering the association of RBPs with human genetic disorders (Gebauer *et al.*, 2021), our work should pave the way to support further studies on the role of RBPs in other immune-related disease settings.

Limitations of the study

To reduce false positive calls of RBP interaction, we have used a very stringent cut-off of LFC>4. This cut-off does by no means mean that a cut off <4 is not a valid target (as exemplified by ZFP36L2), or that >4 is *per se* an RBP interacting with the cytokine mRNAs. All identified RBPs require further validation. Furthermore, the non-crosslinking approach applied here for the RNA aptamer pulldown and the RIP assays may select for high-affinity RNA-RBP interactions, and weak interactions with RNA may therefore remain undetected. Irrespective of this restriction, we identify >100 RBPs interacting with cytokine 3'UTRs. This high number of identified RBPs could stem from heterogeneity of RBP-RNA interactions between different T cells, or from heterogeneous binding to specific mRNAs within the same T cell. It may thus reflect a broad spectrum of mRNA-RBP interactions that are possible in the T cells.

Acknowledgements

We thank the animal caretakers of the NKI and the Sanquin FACS facility. We thank G. Stoecklin (University of Heidelberg) for the 4xS1m aptamer construct; T. Schumacher (Netherlands Cancer Institute) for providing MART-1 TCR viral supernatants and Mel526 and Mel888 tumor cell lines; S. van der Burg (Leiden University) for providing 2A14 cell line; M. Hoogenboezem, N. Zandhuis and S. Castenmiller for technical help and D. Amsen and M. Nolte for critical reading of the manuscript.

This research was supported by Dutch Cancer Society (KWF Kankerbestrijding, grant 10132), European Research council (ERC) consolidator award PRINTERS 817533 and Oncode Institute, all to M.C.W., and the Amsterdam Infection and Immunity (AII) Extension Grant for Postdocs (25262) to B.P.

Author contributions

B.P., F.S. and M.C.W. designed experiments. B.P., A.G., S.E., A.P.J., N.P., J.J.F.H., F.P.J.v.A., F.S., M.C.W. performed experiments. B.P., B.P.N., A.P.J., M.v.d.B., F.P.J.v.A, and M.C.W. analyzed the data. B.P. and M.C.W. wrote the manuscript. M.C.W. supervised the project.

Declaration of interests

The authors declare no competing interests.

Figure legends

Figure 1. 3'UTR-mediated regulation of protein production in murine and human $CD8^+$ T cells

(A) OT-I T cells were transduced with indicated GFP reporter constructs. The empty GFP construct was used as control. (top) Representative GFP expression levels of resting T cells (gray histograms), and of T cells activated with $OVA_{257–264}$ peptide for 6 and 16 h (dashed and solid black lines, respectively). (bottom) Fold increase of GFP gMFI upon activation with $OVA_{257–264}$ peptide compared to resting GFP-expressing OT-I T cells. Data depict mean ± s.d. of 3-4 mice, compiled from 2 independently performed experiments. Each dot represents 1 mouse.

(B) Human T cells were transduced with GFP reporter constructs containing human 3'UTRs, or with GFP empty control. (top) Representative GFP expression levels of $CD8^+$ T cells that were non-activated (gray histograms), or that were activated with PMA/Ionomycin (PMA/I) for 6 and 16 h (dashed and solid black lines, respectively). (bottom) Fold increase of GFP gMFI upon activation with PMA/I compared to resting GFP-expressing human $CD8^+$ T cells. Data are presented as mean ± s.d. of 3 donors, and are representative of 2 independently performed experiments. B, C: one-way ANOVA with Dunnett's multiple comparison to the control; *P < 0.05; **P < 0.01; ***P < 0.001; ****P < 0.0001.

Figure 2. Identification of RNA binding proteins that interact with *IFNG*, *TNF* and *IL2* 3'UTRs.

(A) Schematic representation of the RBP pull-down assay. T cells from 40 pooled donors were activated for 2 days with α-CD3/α-CD28 and rested for 5 days in the presence of rhIL-2. Lysates were incubated with *in vitro* transcribed cytokine 3'UTR-containing 4xS1m RNA aptamers, or with empty 4xS1m RNA aptamers (control). Proteins binding to 4xS1m RNA aptamers were identified by label-free MS analysis.

(B) Heatmap of RBPs that were reproducibly enriched upon pull-down with 4xS1m RNA aptamers containing the *IFNG*, *TNF* or *IL2* 3'UTR, compared to empty control (n=138). Each lane depicts one replicate. Enrichment cut-off was LFC>4. Color scale of heatmaps represents Z-scored log2 median-centered intensities. Gray: not detected.

(C) Representative biological processes that were enriched among the identified RBPs from (B) (Fisher's Exact with FDR multiple test correction).

(D) Comparison of protein raw log2 median-centered intensities from *IFNG* (left panel), *TNF* (middle panel) and *IL2* (right panel) pull-down versus empty control. Expression levels of duplicates (*IFNG*) or triplicates (*TNF* and *IL2*) were averaged. Purple dots depict RBP candidates that were identified in one pull-down experiment with enrichment LFC>4 compared to empty control, and green dots denote RBP candidates that were reproducibly identified in at least 2 independently performed pull-down experiments, each with T cells pooled from 40 donors. Gray dots depict all proteins identified in the experiment shown. n.d.= not detected.

Figure 3. The RBP landscape of *IFNG*, *TNF* and *IL2* 3'UTR alters upon T cell activation.

(A) Heatmap of reproducibly enriched RBPs from cytosolic lysates of PMA/I-activated T cells (2 h) upon pull-down with cytokine 3'UTR-containing 4xS1m aptamers compared to empty 4xS1m aptamers (control) (n=77; right lanes). RBPs enriched from resting T cell lysates that derived from paired samples (Fig. 2B) were included for comparison (left lanes). Enrichment cut-off: LFC>4. Each lane depicts one replicate. Color scale of heatmaps represents Z-scored log2 median-centered intensities. Gray: not detected.

(B) Representative biological processes enriched among the RBPs that were reproducibly identified from activated T cells (Fisher's Exact with FDR multiple test correction).

(C) Comparison of protein raw log2 median-centered intensities from *IFNG* (left panel), *TNF* (middle panel) and *IL2* (right panel) 3'UTR pull-downs from rested T cells versus activated T cells.

(D) Log2 Fold Change (LFC) of log2 intensities from *IFNG* (left panel), *TNF* (middle panel) and *IL2* (right panel) 3'UTR pull-down between rested and activated T cells and LFC of protein log2 intensities from the full proteome of the cytosolic lysates between rested and activated T cells.

(C, D) Expression levels of triplicates were averaged. Green and purple dots show proteins with enrichment LFC>4 compared to control and LFC<-4 or >4 between rested and activated T cells. Purple dots depict RBP candidates identified in one pull-

down experiment, green dots denote RBP candidates reproducibly identified in at least 2 independently performed pull-down experiments, each with T cells pooled from 40 donors. Gray dots depict all proteins identified in one experiment. n.d.= not detected.

Figure 4. ZFP36L1 dampens the production of IFN-γ, TNF and IL-2 in human T cells.

(A) Native RNA immunoprecipitation (RIP) with α-ZFP36L1 antibody from cytosolic lysates of human T cells activated for 2 h with PMA/I. IgG isotype was used as control. (top) Enrichment of ZFP36L1 upon RIP, as determined by immunoblot. (bottom) ZFP36L1 interaction with endogenous *IFNG*, *TNF* and *IL2* mRNA was determined by qRT-PCR. Compiled data of 2 donors from 2 independently performed experiments, data are represented as mean ± s.d.

(B) (left) ZFP36L1 KO efficiency measured with immunoblot in primary human T cells 7 days after nucleofection with Cas9/crRNAs targeting ZFP36L1. Non-targeting crRNA was used as control. (right) Representative IFN-γ, TNF and IL-2 protein expression by ZFP36L1-deficient and control $CD8^+$ T cells after 4h reactivation with α-CD3/α-CD28. Brefeldin A was added for the last 2h. Data are representative of at least 4 independent experiments, each with 1-3 donors (see Figure 4C).

(C-E) IFN-γ, TNF, and IL-2 protein production kinetics of ZFP36L1 KO (red) and control (black) $CD8^+$ T cells stimulated with α-CD3/α-CD28 for indicated time points. Brefeldin A was added for the last 2h of activation (for the 1h time point: from the beginning).

(C) Representative IFN-γ and TNF protein expression by ZFP36L1 KO and paired control $CD8^+$ T cells.

(D) Percentage and gMFI of cytokine producing $CD8^+$ T cells. Data are presented as mean ± s.d. of 3 donors and representative of at least 2 independent experiments. Ratio paired t test (*P <0.05; **P<0.01).

(E) Fold increase of percentage (top) and gMFI (bottom) of cytokine production in ZFP36L1 KO and paired control T cells at 8h after reactivation with α-CD3/α-CD28. Compiled data of 6 donors from 2 independently performed experiments. Unpaired t test (*P <0.05; **P<0.01; ***P<0.001; ****P < 0.0001).

(F) *IFNG*, *TNF* and *IL2* mRNA levels of ZFP36L1 KO and control T cells that were reactivated with α-CD3/α-CD28 for 3h and then treated with Actinomycin D (ActD) for indicated time points. Data are presented as mean ± s.d. of 3 donors and representative of 2 independently performed experiments. Unpaired t test (*P <0.05; **P<0.01).

(G) Cytokine mRNA levels of ZFP36L1 KO and control T cells that were reactivated for indicated time points with α-CD3/α-CD28. Data are presented as mean ± s.d. of 3 donors and representative of 2 independently performed experiments. Ratio paired t test (*P <0.05; **P<0.01).

(H) Co-immunoprecipitation with α-ZFP36L1 antibodies or IgG control from cytosolic lysates of 2h PMA/I-activated human T cells, followed by MS analysis. Data represent protein raw log2 median-centered intensities from ZFP36L1 immunoprecipitation versus IgG control. Expression levels of biological replicates were averaged (n=3 donors). Green dots depict putative interactors of ZFP36L1 that were identified with cut-off LFC>6 compared to IgG control. Gray dots depict all proteins identified in one experiment. n.d.= not detected.

Figure 5. ZC3HAV1, ATXN2L and HuR modulate cytokine production in human T cells.

(A) (top) KO efficiency of indicated RBPs in human T cells 7 days after CRISPR/Cas9 gene-editing. Non-targeting crRNA was used as control. (bottom) IFN-γ and TNF protein expression after 4h of activation with α-CD3/α-CD28. Brefeldin A was added for the last 2h. Data are representative of at least 2 independent experiments, each with 3 donors (see Figure 5C).

(B) Native RNA immunoprecipitation (RIP) with antibodies specific for ATXN2L, ZC3HAV1 or HuR from cytosolic lysates of human T cells activated with PMA/I for 2h (or 1h for HuR). IgG isotype was used as control. (top) Enrichment of indicated RBP upon RIP, as determined by immunoblot. (bottom) RBP interaction with endogenous cytokine mRNA was determined by qRT-PCR. Compiled data of 3 donors for ATXN2L and HuR and 2 donors for ZC3HAV1, from 2-3 independently performed experiments, presented as mean ± s.d. Unpaired t test when RIP was performed with 3 donors (*P <0.05; **P<0.01;).

(C) IFN-γ, TNF, and IL-2 protein production kinetics of human RBP KO $CD8^+$ T cells stimulated with α-CD3/α-CD28 for indicated time points. Data are presented as mean ± s.d. of 3 donors and representative of at least 2 independent experiments. Ratio paired t test (*P <0.05; **P<0.01, ****P < 0.0001).

(D) Fold increase of % of cytokine production in human RBP KO T cells compared to control. Compiled data of 6 donors from 2 independently performed experiments. Unpaired t test (*P <0.05; ***P<0.001 ****P < 0.0001).

Figure 6. RBPs regulate cytokine expression in tumor-specific human T cells.

(A) MART1 TCR-engineered T cells were CRISPR/Cas9 gene-edited for indicated RBP, or treated with non-targeting crRNA as control. Representative dot plots of cytokine production after 6h of co-culture with $MART1^+$ tumor cells. Brefeldin A was added for the last 2h. Data are representative of at least 2 independent experiments, each with 3-4 donors.

(B) Compiled data of 7 donors after 6 and 24 h of stimulation with $MART1^+$ tumor cells from 2 independently performed experiments. Data are presented as mean ± s.d. Ratio paired t test (*P <0.05).

(C) Graphs depict the cytokine profile analysis of MART1-specific $CD8^+$ T cells. Data are presented as mean ± s.d. of 3 donors and representative of at least 2 independent experiments.

(D) Representative dot plots of IFN-γ and TNF production after 6 h of co-culture with $MART1_{26-35}$ peptide-loaded 2A14 tumor cells. Brefeldin A was added for the last 2h of activation. Data are representative of at least 2 independent experiments, each with 3 to 5 donors.

(E) Compiled data of 8 donors after 6 h of stimulation with MART1-loaded 2A14 tumor cells from 2 independently performed experiments. Data are presented as mean ± s.d. Ratio paired t test (*P <0.05; **P<0.01; ***P<0.001).

Figure 7. ZFP36L1 dampens cytokine production in tumor-specific T cells *in vivo*.

(A) $Ly5.1^+$ C57BL/6J mice were engrafted with B16-OVA tumors. 7 days later when tumors reached a size of ~ 4-8 mm^2, mice received $1x10^6$ control or Zfp36l1 KO OT-I $Ly5.2^+$ T cells. 14 days after T cell transfer, tumors were excised and tumor-infiltrating T cells (TILs) were analyzed.

(B) Absolute numbers of control and Zfp36l1 KO OT-I TILs per gram of tumor. Unpaired t test.

(C) (left) Representative IFN-γ protein expression by control or Zfp36l1-deficient OT-I TILs *ex vivo* with or without reactivation with 100nM $OVA_{257–264}$ peptide for 4 h, brefeldin A and monensin added for the last 2 h. (right) Percentage of gMFI of IFN-γ producing OT-I $CD8^+$ T cells. Data are presented as mean ± s.d. with n=7, and are representative of 2 independent experiments. Unpaired t test (*P <0.05; **P<0.01).

(D) (left) Representative CD107a and Granzyme B expression by control and Zfp36l1-deficient OT-I TILs *ex vivo* in the presence of brefeldin A and monensin for 2 h. (right) Zfp36l1-deficient and control OT-I T cells reactivated with 100nM $OVA_{257–264}$ peptide for 4 h, or left untreated, in the presence of brefeldin A and monensin for the last 2h. Data are presented as mean ± s.d. with n=7 and representative of 2 independent experiments. Unpaired t test (**P<0.01; ***P<0.001).

(E) Tumor size of $Ly5.1^+xLy5.2^+$ F1 B16-OVA tumor-bearing mice treated with 0.65 x 10^6 Zfp36l1 KO or control OT-I $Ly5.2^+$ T cells at day 7 after tumor injection. Dashed line represents time point of 14 days after the T cell transfer. n = 8 mice/group.

(F) Tumor size of tumor-bearing mice at day 21 (14 days after the T cell transfer). n = 8 mice/group. Unpaired t test (*P<0.05).

Supplementary figure legends

Figure S1. Cytokine 3'UTRs define the protein production in $CD8^+$ and $CD4^+$ T cells

(A-E) GFP fluorescence measured by flow cytometry in T cells transduced with GFP-3'UTR constructs.

(A) GFP gMFI in resting mouse $CD8^+$ T cells. Data depict the mean ± s.d. of 3-4 mice, compiled from 2 independently performed experiments (one-way ANOVA with Dunnett's multiple comparison to the control; ***P < 0.001; ****P < 0.0001).

(B) GFP gMFI in resting human $CD8^+$ T cells or

(C) human $CD4^+$ T cells. Data are presented as mean ± s.d. of 3 donors and representative of at least 2 independently performed experiments (one-way ANOVA with Dunnett's multiple comparison to the control; *P < 0.05; **P < 0.01; ***P < 0.001).

(D-E) (top) Representative GFP expression levels of human $CD8^+$ T cells (D) and $CD4^+$ T cells (E) left untreated (resting, gray histograms), or that were reactivated for 6 and 16 h (dashed and solid black lines, respectively). (bottom) Fold increase of GFP gMFI upon reactivation compared to resting GFP-expressing $CD8^+$ T cells (D) and $CD4^+$ T cells (E). Data are presented as mean ± s.d. of 3 donors and representative of at least 2 independently performed experiments (one-way ANOVA with Dunnett's multiple comparison to the control; *P < 0.05; **P < 0.01; ***P < 0.001; ****P < 0.0001).

Figure S2. Mass spectrometry analysis of RBP pull-downs with 4xS1m RNA aptamers containing the *IFNG*, *TNF* or the *IL2* 3'UTR.

(A-B) Mass spectrometry analysis of RBP pull-downs from resting T cells. Replicate 2 from *IFNG* 3'UTR samples is outlined (dashed red line, and Fig S2B) and excluded from further analysis due to the non-normal distribution of data.

(A) Number of proteins identified by MS analysis per sample (bars) and of all 12 samples combined after filtering (red line; n = 1,808). Sample indicated with dashed line shows less protein identification.

(B) Data distribution plot of protein log2 intensities per sample. Sample indicated with dashed line shows altered data distribution and was therefore excluded from the analysis.

(C) Number of proteins identified from 2 h PMA/Ionomycin activated T cells by MS analysis per sample (bars) and of all 12 samples combined after filtering (red line; n = 1,596).

(D) Protein raw log2 intensities from *IFNG*, *TNF* and *IL2* 3'UTR pull-downs and from full proteome of rested T cells versus activated T cells with PMA/I. Each dot represents one replicate. Data are represented as mean ± s.d. LFC = log2 fold change, n.d.= not detected.

Figure S3. Regulation of IFN-γ, TNF and IL-2 production in human T cells by ZFP36L1.

(A) Representative IFN-γ, TNF and IL-2 protein expression in ZFP36L1-deficient and control $CD8^+$ T cells rested for 7 d. Brefeldin A was added for 2 h. Data are representative of at least 4 independent experiments, each with 1 to 3 donors.

(B) Fold increase of % (left) and gMFI (right) of cytokine production in ZFP36L1 KO T cells compared to control at 4 h after reactivation with α-CD3/α-CD28, with brefeldin A for the last 2 h. Compiled data with n=6 from 2 independently performed experiments. Unpaired t test (*P <0.05; ***P < 0.001; ****P < 0.0001).

(C) IFN-γ and IL-2 production kinetics of ZFP36L1 KO and control $CD8^+$ T cells stimulated with α-CD3/α-CD28 for indicated time points. Brefeldin A was added for the last 2 h of activation (or from the beginning for the 1 h time point). Representative dot plots as determined by intracellular cytokine staining. Data are representative of at least 6 donors from 2 independent experiments.

(D) ZFP36L1 expression in $CD8^+$ T cells stimulated with α-CD3/α-CD28 for indicated time points.

(E) IFN-γ, TNF, and IL-2 production kinetics shown as percentages and gMFI of ZFP36L1 KO and control $CD4^+$ T cells stimulated with α-CD3/α-CD28 for indicated time points. Brefeldin A was added for the last 2 h (or from the beginning for 1 h time point). Data are presented as mean ± s.d. of 3 donors and representative of 2 independently performed experiments. Ratio paired t test (*P <0.05; **P<0.01).

(F) Mass spectrometry analysis of co-immunoprecipitation with α-ZFP36L1 or IgG from activated T cell lysates. Number of proteins identified by MS analysis per sample (bars) and of all 6 samples combined after filtering. The analysis identified in total 1636 proteins with an LFC>6 (red line) in all 3 biological replicates of at least one condition.

Figure S4. RBP-mediated regulation of cytokine production in human T cells

(A) IFN-γ and IL-2 production kinetics of resting RBP KO and control $CD8^+$ T cells stimulated with α-CD3/α-CD28 for indicated time points. Brefeldin A was added for the last 2 h (or from the beginning for the 1 h time point). Representative dot plots as determined by intracellular cytokine staining. Data are representative of at least 6 donors from 2 independent experiments.

(B) Cytokine production kinetics shown as gMFI of RBP KO $CD8^+$ T cells stimulated with α-CD3/α-CD28 for indicated time points. Data are presented as mean ± s.d. of 3 donors and representative of at least 2 independently performed experiments. Ratio paired t test (*P <0.05; **P<0.01).

(C) Cytokine production kinetics of RBP KO and control $CD4^+$ T cells stimulated with α-CD3/α-CD28 for indicated time points. Data are presented as mean ± s.d. of 3 donors and representative of at least 2 independently performed experiments. Ratio paired t test (*P <0.05; ***P < 0.001).

Figure S5. Cytokine mRNA expression is not affected by RBPs ZC3HAV1, ATXN2L and HuR in activated human T cells.

(A) *IFNG*, *TNF* and *IL2* mRNA levels of RBP KO and control T cells rested for 7 d reactivated with α-CD3/α-CD28 for 3 h (ZC3HAV1 KO and ATXN2L KO) or 1h (HuR KO) and then treated with Actinomycin D (ActD) for 60 and 120 min. Data are presented as mean ± s.d. of 3 donors and representative of 2 independently performed experiments. Unpaired t test.

(B) *IFNG*, *TNF* and *IL2* mRNA levels of RBP KO and control T cells that were activated with α-CD3/α-CD28 for indicated time points. Cytokine mRNA levels in HuR KO T cells were determined at 1-3 h after activation and mRNA levels in ZC3HAV1 KO and ATXN2L KO were determined at 3-5 h after activation. Data are presented as mean ± s.d. of 3 donors and representative of 2 independently performed experiments. Ratio paired t test.

Figure S6. Antigen-dependent regulation of cytokines per cell expression by RBPs in human T cells.

(A) MART1 TCR-engineered T cells were depleted from indicated RBP by CRISPR/Cas9 gene-editing, or treated with non-targeting crRNA as control. RBP KO efficiency was measured with immunoblot 7 days after nucleofection.

(B) Representative dot plots of cytokine production by MART1-specific control T cells after 6 h of co-culture with $MART1^+$ Mel526 or $MART1^-$ Mel888 tumor cells. Brefeldin A was added for the last 2 h of activation. Data are representative of at least 2 independent experiments, each with 3-4 donors.

(C) IFN-γ, TNF, and IL-2 production shown as gMFI of RBP KO and control $CD8^+$ T cells after 6 h of stimulation with MART1-loaded 2A14 tumor cells. Compiled data of 8 donors from 2 independently performed experiments. Data are presented as mean ± s.d. Ratio paired t test (*P <0.05; **P<0.01; ***P<0.001).

Figure S7. ZFP36L1 dampens cytokine production in tumor-specific T cells *in vivo*.

(A-D) Ly5.1^{+} C57BL/6J mice were engrafted with B16-OVA tumors. 7 days later when tumors reached a size of ~ 4-8mm^{2}, mice received 1x10^{6} Zfp36l1 KO or control OT-I Ly5.2^{+} T cells. 14 days after T cell transfer, tumors and spleens were excised and OT-I T cells were analyzed.

(A) Zfp36l1 KO efficiency measured with immunoblot 2 days after nucleofection with RNP targeting Zfp36l1. Non-targeting crRNA was used as control.

(B) Cytokine expression by Zfp36l1-deficient and control OT-I TILs,

(C) or by splenic OT-I T cells *ex vivo* with or without reactivation with 100nM $OVA_{257–264}$ peptide for 4 h in the presence of brefeldin A and monensin for the last 2 h. Data are presented as mean ± s.d. with n=7 and representative of 2 independent experiments. Unpaired t test (*P <0.05; **P<0.01).

(D) CD107a and Granzyme B expression by Zfp36l1-deficient and control splenic OT-I T cells. Data are presented as mean ± s.d. with n=7 and representative of 2 independent experiments. Unpaired t test.

Methods

Cloning and preparation of *in vitro* transcribed S1m aptamers

Gene-specific full length 3′UTRs were amplified from genomic DNA of a C57BL/6J mouse or from human genomic DNA. Human and mouse 3′ UTR variants were cloned into the BamHI and NotI sites of pRETRO-SUPER GFP (Table S6) (Brummelkamp *et al.*, 2002) downstream of GFP, all under the control of the murine Pgk1 promoter. 4xS1m RNA aptamers containing the full length 3'UTR of human *IFNG*, *TNF* and *IL2* were cloned into the pSP73-4xS1m vector (Leppek *et al.*, 2014) as previously described (Salerno *et al.*, 2018). All sequences were confirmed by Sanger sequencing. To generate 4xS1m RNA aptamers alone or containing the human *IFNG* 3′ UTR, *IL2* 3′ UTR and *TNF* 3′ UTR, plasmids were linearized with NdeI, *in vitro* transcribed using the Ampliscribe T7-flash transcription kit (Epicentre), and RNA was purified using the mini Quick Spin Oligo columns (Roche). The RNA quality and quantity was determined by RNAnano Chip assay (Agilent).

Mice

C57BL/6J/Ly5.1 mice, C57BL/6J/Ly5.1/Ly5.2 mice and C57BL/6J.OTI T cell receptor (TCR) transgenic mice (OT-I) mice were bred in-house at the Netherlands Cancer Institute (NKI). Experiments were performed in accordance with institutional and national guidelines and approved by the Experimental Animal Committee at the NKI. All animals were housed in individually ventilated cage systems under specific-pathogen-free conditions. Mice were used at 6-12 weeks of age.

T cell activation and culture

Studies with human T cells from anonymized healthy donors were performed in accordance with the Declaration of Helsinki (Seventh Revision, 2013) after written informed consent (Sanquin). Peripheral blood mononuclear cells (PBMCs) were isolated through Lymphoprep density gradient separation (Stemcell Technologies). Cells were used after cryopreservation. Human T cells were activated as previously described (Nicolet *et al.*, 2020). Briefly, 24-well plates were pre-coated overnight with 0.5 µg/mL rat α-mouse IgG2a (clone MW1483, Sanquin) at 4 ºC. Plates were washed once with PBS, coated with 1 µg/mL α-CD3 (clone Hit3a, Biolegend) for a minimum of 4 h at 37 ºC. $1x10^6$ PBMCs/well were seeded with 1 µg/mL α-CD28

(clone CD28.2, Biolegend) in 1 mL IMDM (Lonza) supplemented with 10 % fetal bovine serum (FBS, Bodinco), 100 U/mL Penicillin, 100 µg/mL streptomycin and 2 mM L-glutamine (all Sigma-Aldrich). After 48 h of incubation at 37 °C, 5 % CO_2, cells were harvested and further cultured in standing T25/75 tissue culture flasks (Thermo Scientific) at a density of 0.8×10^6/mL in IMDM supplemented with 5 % heat-inactivated human serum (Sanquin), 5 % FBS and 100 IU/mL recombinant human (rh) IL-2 (Proleukin, Clinigen). Medium was refreshed every 3 days. For nucleofection, T cells were cultured in T-cell mixed media (Miltenyi) supplemented with 5 % heat-inactivated human serum, 5 % FBS, 100 U/mL Penicillin, 100 µg/mL streptomycin, 2 mM L-glutamine, 100 IU/mL rhIL-2 and 10 ng/mL rhIL-15 (Peprotech).

Mouse splenic OT-I T cells were purified with the $CD8a^+$ T Cell Isolation Kit (Miltenyi Biotec) according to the manufacturer's protocol. $1x10^6$ OT-I T cells were cultured for 20 h with $1x10^5$/well pre-seeded MEC.B7.SigOVA cells (van Stipdonk *et al.*, 2003) at 37 °C and 5 % CO_2 in IMDM containing 10% FBS, 100 U/mL Penicillin, 100 µg/mL streptomycin, 2 mM L-glutamine and 15 µM 2-mercaptoethanol. Cells were harvested, washed and maintained with 10 ng/ml recombinant mouse (rm) IL-7 (Peprotech).

Retroviral transduction

For virus production, FLYRD18 (ECACC 95091902) cells for human and Plat-E cells (Morita *et al.*, 2000) for mouse T cells were used. Both packaging cell lines were cultured at 37 °C and 5 % CO_2 in IMDM supplemented with 10 % FBS, 100 U/mL Penicillin, 100 µg/mL streptomycin and 2 mM L-glutamine. Virus packaging cells were plated into 6-well plates at 5-6 x 10^5 cells per well. Next day, cells were transfected with 1 µg of retroviral vector using GeneJammer (Agilent), according to the manufacturer's protocol. After 48 h, virus supernatant was harvested, filtered through a 0.45 µm filter and stored at -80 °C. For retroviral transduction of human T cells, PBMCs from individual donors were activated for 48 h with α-CD3/α-CD28 as described above. Transduction was performed with Retronectin (Takara) as described (Nicolet *et al.*, 2020). Briefly, non-tissue culture treated 24-well plates were coated with 50 µg/mL Retronectin overnight at 4 °C and washed once with PBS. Subsequently, 300-500 µL viral supernatant was added per well and was centrifuged for 30 min at 4 °C at 4500 rpm (2820 g). $1x10^6$ freshly activated T cells were added

per well, spun for 5 min at 1000 rpm (180 g), and cultured at 37 °C and 5 % CO_2 in a humidified incubator. Cells were refreshed after 24 h and cultured in standing T25/75 flasks at a concentration of $0.8x10^6$ cells/mL for 5 to 14 days in presence of rhIL-2 and rhIL-15. Medium was refreshed every 3 days.

For retroviral transduction of mouse T cells, preactivated $CD8^+$ OT-I T cells were harvested and retrovirally transduced as described above. T cells were maintained with 10 ng/ml rm IL-7 and reactivated with 100 nM $OVA_{257–264}$ peptide (Genscript).

4xS1m RNA aptamer-protein pull-down

α-CD3/α-CD28 activated human T cells were cultured for 5 days. T cells that were activated with PMA/Ionomycin for 2 h or left untreated were washed twice with ice-cold PBS, and the cell pellet was snap frozen in liquid nitrogen. Cells were homogenized using 5-mm steel beads and a tissue lyser (Qiagen TissueLyser II) 6x at 25 Hz for 15 s. The homogenate was then solubilized and precleared as previously described (Salerno *et al.*, 2018). Cell lysates were incubated with RNA-aptamer-coupled beads for 3.5 h at 4 °C under rotation in the presence of 60 U RNasin (Ambion). For each pull-down, about 30 µg of *in vitro* transcribed RNA, coupled to Streptavidin Sepharose High Performance beads (GE Healthcare), and 5-10 mg cell lysate protein was used. RNA-bound proteins were eluted by adding 1 µg RNaseA (Thermo Scientific) in 100 µl 100 mM Tris-HCl, pH 7.5 (Gibco-Invitrogen). Proteins were reduced, alkylated and digested into peptides using trypsin (Promega). Peptides were desalted and concentrated using Empore-C18 StageTips and eluted with 0.5 % (v/v) acetic acid, 80 % (v/v) acetonitrile. Sample volume was reduced by SpeedVac and supplemented with 2 % acetonitrile and 0.1 % TFA.

Co-immunoprecipitation

Cytoplasmic lysates of human T cells activated for 2 h with PMA/Ionomycin ($100x10^6$ cells per condition) were prepared using lysis buffer (140 mM NaCl, 5 mM $MgCl_2$, 20 mM Tris/HCl pH7.6, 1 % Digitonin) that was freshly supplemented with 1% of protease inhibitor cocktail (Sigma). Protein A Dynabeads (Invitrogen) were prepared according to the manufacturer's protocol. The lysate was immunoprecipitated for 4 h at 4 °C with 10 µg polyclonal rabbit α-ZFP36L1 (ABN192, Sigma-Aldrich) or with a polyclonal rabbit IgG isotype control (12-370, Sigma-Aldrich). Beads were washed twice with wash buffer (150 mM NaCl, 10 mM Tris/HCl pH7.6, 2 mM EDTA,

protease/phosphatase inhibitor cocktail), and then twice with 10 mM Tris/HCl pH7.6. Immunoprecipitated proteins were reduced and alkylated on-beads. Proteins were detached from the beads by incubation with 250 ng trypsin for 2 h at 20 °C. Beads were removed and proteins were further digested into peptides with 350 ng trypsin for 16 h. Peptides were prepared for MS analysis, as described above.

Mass spectrometry data acquisition.

Tryptic peptides were separated by nanoscale C18 reverse chromatography coupled online to an Orbitrap Fusion Tribrid mass spectrometer via a NanoElectroSpray Ion Source (both Thermo Scientific). Peptides were loaded on a 20 cm 75-360 µm inner-outer diameter fused silica emitter (New Objective) packed in-house with ReproSil-Pur C18-AQ 1.9 µm resin (Dr Maisch GmbH). The column was installed on a Dionex Ultimate3000 RSLC NanoSystem (Thermo Scientific) using a MicroTee union formatted for 360 µm outer diameter columns (IDEX) and a liquid junction. The spray voltage was set to 2.15 kV. Buffer A was composed of 0.5 % acetic acid and buffer B of 0.5 % acetic acid, 80 % acetonitrile. Peptides were loaded for 17 min at 300 nl/min at 5 % buffer B, equilibrated for 5 min at 5 % buffer B (17-22 min) and eluted by increasing buffer B from 5 to 15 % (22-87 min) and 15 to 38 % (87-147 min), followed by a 10 min wash to 90 % and a 5 min regeneration to 5 %. Survey scans of peptide precursors from 400 to 1,500 m/z were performed at 120 K resolution (at 200 m/z) with a 4×10^5 ion count target. Tandem mass spectrometry was performed by isolation with the quadrupole with isolation window 1.6, HCD fragmentation with normalized collision energy of 30 and rapid scan mass spectrometry analysis in the ion trap. The MS2 ion count target was set to 10^4 and the maximum injection time was 35 ms. Only those precursors with charge states 2-7 were sampled for MS2. The dynamic exclusion duration was set to 30 s with a 10-p.p.m. tolerance around the selected precursor and its isotopes. Monoisotopic precursor selection was turned on. The instrument was run in top speed mode with 3 s cycles. All data were acquired with Xcalibur software.

Mass spectrometry data analysis.

The raw mass spectrometry files were processed with the MaxQuant computational platform, 1.6.2.10 (Cox *et al.*, 2008). Proteins and peptides were identified using the Andromeda search engine by querying the human Uniprot database (downloaded

February 2017 and February 2019, 89,796 entries) for the RNA pull-down. Standard settings with the additional options match between runs, and unique peptides for quantification were selected. The generated 'proteingroups.txt' data were imported in R and processed with the Differential Enrichment analysis of Proteomics data (DEP) R package (Zhang *et al.*, 2018). Identified peptides were filtered for potential contaminants, only identified by site and reverse hits. The raw intensity values were transformed in log2 scale and averaged, and log2 fold change (LFC) was calculated. To identify enriched proteins, we used a cut-off of LFC> 4, compared to empty aptamer control. We only included proteins that were idenitifed in at least 2 out of 3 replicates in this analysis. To select for RBPs, we compiled the 1153 RBPs identified by RNA-interactome capture on HeLa and Jurkat cells (Castello *et al.*, 2016; Perez-Perri *et al.*, 2018) with 1542 computationally predicted RBPs based on the presence of a defined list of RNA-binding domains (RBDs) (Gerstberger *et al.*, 2014), resulting in a list of 2026 unique RBPs (Table S7). Filtered data are shown as log2 median-centered intensities. The MS data of the aptamer pulldown and the co-IP have been deposited to the ProteomeXchange Consortium via the PRIDE partner repository with the dataset identifier PXD028171.

GO analysis

Gene ontology analysis was performed with the Panther database (version 16.0)(Mi *et al.*, 2019). A statistical overrepresentation test (Fisher's exact with FDR multiple test correction) was performed with a reference list composed of all *Homo Sapiens* genes in the database. Overrepresented GO terms (FDR<0.001) were filtered for RNA-related functions and manually curated. Due to space constrains, only selected terms were included in the main figures. Full lists of overrepresented GO terms are provided in Table S2 and Table S4**.** The R package ggplot2 was used to generate the graphical representations.

crRNA design

crRNAs were designed using the CRISPR design tools in Benchling (https://benchling.com, Table S6). Sequences were verified to be specific for the target of interest via BlastN (NCBI).

Genetic modification of T cells with Cas9 RNPs

Cas9 RNP production and T cell nucleofection was performed as previously described (Freen-van Heeren *et al*., 2020). Briefly, Alt-R crRNA and ATTO550-labeled tracr-RNA were reconstituted to 100 µM in Nuclease Free Duplex buffer (Integrated DNA Technologies). Non-targeting control was used as a negative control (Integrated DNA Technologies). Oligos were mixed at equimolar ratios (i.e. 4.5 µL crRNA + 4.5 µL tracrRNA) and denatured by heating at 95 ºC for 5min in a thermocycler. Nucleic acids were cooled down to room temperature prior to mixing them with 30 µg TrueCut Cas9 V2 (Invitrogen) to produce Cas9 ribonuclear proteins (RNPs). Mixture was incubated at room temperature for at least 10min prior to nucleofection. For nucleofection, $1*10^6$ T cells were activated for 72 h with α-CD3/α-CD28 in complete T-cell mixed media. Mouse splenic OT-I T cells were activated for 20 h MEC.B7.SigOVA cells (van Stipdonk, 2003) and rested for 24 h in medium with IL-7 prior to nucleofection. Cells were harvested, washed with PBS and $3x10^6$ cells were resuspended in 20 µL P2 Buffer (Lonza). Cas9 RNPs were added and incubated for 2 min. Cells were then electroporated in 16-well strips in a 4D Nucleofector X unit (Lonza) with program EH-100 for human T cells, and with program CM137 for mouse T cells. Cells were transferred to 48-well plates containing prewarmed complete medium and cultured in a humidified incubator at 37 ºC and 5% CO_2. Medium was refreshed every 2-3 days. Nucleofection efficiency was determined on day 2 after electroporation by measuring ATTO550 expression using FACSymphony (BD Biosciences). Knockout efficiency was determined on day 7-10 after electroporation by Western blot as described below.

Quantitative PCR analysis

Total RNA was extracted using Trizol (Invitrogen) and cDNA was synthesized with SuperScript III (Invitrogen). RT-PCR was performed with duplicate reactions using SYBR Green on a StepOne Plus (both Applied Biosystems). Ct values were normalized to 18S levels (Nicolet *et al.*, 2017).

To determine the half-life of cytokine mRNA, T cells were activated for indicated timepoint (1 or 3 h) with α-CD3 and α-CD28, and then treated with 5 µg/ml actinomycin D (ActD) (Sigma-Aldrich).

RNA immunoprecipitation and immunoblot

Cytoplasmic lysates of human T cells activated with PMA/Ionomycin ($300x10^6$ cells per condition) were prepared using lysis buffer (10 mM HEPES, pH 7.0, 100 mM KCl, 5 mM MgCl2, 0.5 % NP40) freshly supplemented with 1 mM DTT, 40 U/ml RNase OUT (both Invitrogen), 0.4 mM vanadylribonucleoside complex RNase inhibitor (NEB) and 1 % EDTA-free protease/phosphatase inhibitor cocktail (Thermo Scientific). Protein A or protein G Dynabeads (Invitrogen) were prepared according to the manufacturer's protocol. The lysate was immunoprecipitated for 4 h at 4 °C with 10 µg polyclonal rabbit α-ZFP36L1 (ABN192, Sigma-Aldrich), α-ZC3HAV1 (GTX120134, GeneTex), α-ATXN2L (ab99304, Abcam) or a polyclonal rabbit IgG isotype control (12-370, Sigma-Aldrich) and a mouse monoclonal α-HuR (3A2, Santa Cruz Biotechnology) or a mouse IgG1 kappa Isotype Control (P3.6.2.8.1, eBioscience). RNA was extracted directly from beads by using Trizol, and mRNA expression was measured by RT-PCR as described above. Specificity of the RNA-IP assay was tested by immunoblotting using α-ZFP36L1 (ab42473, Abcam), α-ZC3HAV1, α-ATXN2L (ab99304, Abcam) or α-HuR (3A2, Santa Cruz Biotechnology), followed by mouse monoclonal anti-Rabbit IgG light chain-HRP (ab99697, Abcam) or goat anti-mouse-HRP (1031-05, Southern Biotech).

Cell lysates ($1x10^6$ cells/sample) were prepared by standard procedures. Proteins were separated on a 4-12 % SDS/PAGE and transferred onto a nitrocellulose membrane by iBlot (Thermo). Rabbit polyclonal α-ZFP36L1 (ab42473, Abcam), α-ZC3HAV1 (PA5-31650, Invitrogen), α-ATXN2L (ab99304, Abcam), mouse monoclonal α-HuR (3A2, Santa Cruz Biotechnology) and anti-RhoGDI (MAB9959, Abnova), were used, followed by either goat α-rabbit (4050-05) and goat α-mouse-HRP secondary antibodies (1031-05, both Southern Biotech).

Functional assays

Human T cells were stimulated with 10ng/ml PMA and 1µM Ionomycin (both Sigma-Aldrich) or 1 µg/mL pre-coated α-CD3 and 1 µg/mL soluble α-CD28 for indicated time points. MART1 TCR-transduced T cells were co-cultured with HLA-A*0201$^+$ MART1^{hi} Mel526 (MART1$^+$), HLA-A*0201- MART1^{lo} Mel888 (MART1$^-$) melanoma cell lines (Marincola *et al.*, 1994), or MART1$_{26-35}$ (Genscript) loaded HLA-A*0201$^+$ 2A14 uveal melanoma cell line (kind gift of S. van den Burg, Leiden University), in a 1:1 effector to target (E:T) ratio for indicated time points. 1 µg/mL brefeldin A (BD GolgiPlug, BD

Biosciences) was added as indicated. Non-activated T cells were used as a negative control. All stimulations were performed in medium supplemented with 10 % FBS, 100 U/mL Penicillin, 100 µg/mL streptomycin and 2 mM L-glutamine.

B16 melanoma tumor model

For *in vivo* studies, C57BL/6J/Ly5.1 or C57BL/6J/Ly5.1/Ly5.2 mice were injected subcutaneously with $1x10^6$ B16-OVA cells. On day 7 when tumors reached ~4-8mm^2, 0.65-$1x10^6$ control or Zfp36l1 KO $CD8^+$ OT-I Ly5.2 T cells were injected i.v.. Prior to T cell transfer, dead cells were removed with Lympholyte M gradient (Cedarlane). Tumor infiltrates were analyzed 14 days after T cell transfer. Excised tumors were cut into small pieces and digested with 100 µg/ml DNase I (Roche) and 200 U/ml Collagenase (Worthington) at 37 °C for 30 min. Cells were counted, and incubated with 1 µg/ml brefeldin A alone for 2 h or, when indicated, they were stimulated for 4 h with 100 nM $OVA_{257–264}$ peptide and brefeldin A for the last 2 h of activation. For tumor growth and survival studies, mice were sacrificed when the tumor reached a size of ~100 mm^2.

Flow cytometry and intracellular cytokine staining

For flow cytometric analysis, cells were washed with FACS buffer (PBS, containing 1 % FBS and 2 mM EDTA) and labeled for 20min at 4°C with monoclonal antibodies α-CD4 (clone SK3 and clone RPA-T4), α-CD8 (clone SK1, all BD Biosciences), α-mouse TCR beta (clone H57-597), α-IFN-γ (clone 4S.B3, both eBioscience), α-IL-2 (clone MQ1-17H12, Biolegend) and α-TNF (clone MAb11, Biolegend and BD Biosciences). Mouse T cells were labelled with α-CD8 (53-6.7), α-GzmB (GB11, both BD Biosciences), α-CD45.1 (A20), α-CD45.2 (104), α-IFN-γ (XMG1.2) and α-TNF (MP6-XT22), α-IL-2 (JES6-5H4), α-CD107a (1D4B) (all eBioscience). Dead cells were excluded with Near-IR (Life Technologies). For intracellular cytokine staining, cells were cultured in the presence of 1 µg/mL brefeldin A for indicated timepoints and were fixed and permeabilized with Cytofix/Cytoperm kit (BD Biosciences) according to manufacturer's protocol. Expression levels were acquired using

FACSymphony (BD Biosciences) and data were analyzed using FlowJo (BD Biosciences, version 10).

Statistical analysis

Results are shown as mean ± s.d. Statistical analysis between groups was performed with GraphPad Prism 8 with two-tailed ratio paired or unpaired Student t test when comparing two groups, or with one-way ANOVA test with Dunnett correction when comparing more than two groups. p values <0.05 were considered statistically significant.

References

Adachi, S., Homoto, M., Tanaka, R., Hioki, Y., Murakami, H., Suga, H., Matsumoto, M., Nakayama, K.I., Hatta, T., Iemura, S., *et al.* (2014). ZFP36L1 and ZFP36L2 control LDLR mRNA stability via the ERK-RSK pathway. *Nucleic acids research*, 42(15), pp. 10037–49. doi:10.1093/nar/gku652.

Akira, S. and Maeda, K. (2021). Control of RNA Stability in Immunity. *Annual review of immunology*, 39, pp. 481–509. doi:10.1146/annurev-immunol-101819-075147.

Almeida, J.R., Price, D.A., Papagno, L., Arkoub, Z.A., Sauce, D., Bornstein, E., Asher, T.E., Samri, A., Schnuriger, A., Theodorou, I., *et al.* (2007). Superior control of HIV-1 replication by CD8+ T cells is reflected by their avidity, polyfunctionality, and clonal turnover. *The Journal of experimental medicine*, 204(10), pp. 2473–85. doi:10.1084/jem.20070784.

Bell, S.E., Sanchez, M.J., Spasic-Boskovic, O., Santalucia, T., Gambardella, L., Burton, G.J., Murphy, J.J., Norton, J.D., Clark, A.R. and Turner, M. (2006). The RNA binding protein Zfp36l1 is required for normal vascularisation and post-transcriptionally regulates VEGF expression. *Developmental dynamics : an official publication of the American Association of Anatomists*, 235(11), pp. 3144–55. doi:10.1002/dvdy.20949.

Brummelkamp, T.R., Bernards, R. and Agami, R. (2002). Stable suppression of tumorigenicity by virus-mediated RNA interference. *Cancer cell*, 2(3), pp. 243–7. doi:10.1016/s1535-6108(02)00122-8.

Castello, A., Fischer, B., Frese, C.K., Horos, R., Alleaume, A.-M., Foehr, S., Curk, T., Krijgsveld, J. and Hentze, M.W. (2016). Comprehensive Identification of RNA-Binding Domains in Human Cells. *Molecular Cell*, 63(4), pp. 696–710. doi:10.1016/j.molcel.2016.06.029.

Ciuffreda, D., Comte, D., Cavassini, M., Giostra, E., Bühler, L., Perruchoud, M., Heim, M.H., Battegay, M., Genné, D., Mulhaupt, B., *et al.* (2008). Polyfunctional HCV-specific T-cell responses are associated with effective control of HCV replication. *European journal of immunology*, 38(10), pp. 2665–77. doi:10.1002/eji.200838336.

Coelho, M.A., de Carné Trécesson, S., Rana, S., Zecchin, D., Moore, C., Molina-Arcas, M., East, P., Spencer-Dene, B., Nye, E., Barnouin, K., *et al.* (2017).

Oncogenic RAS Signaling Promotes Tumor Immunoresistance by Stabilizing PD-L1 mRNA. *Immunity*, 47(6), pp. 1083-1099.e6. doi:10.1016/j.immuni.2017.11.016.

Cox, J. and Mann, M. (2008). MaxQuant enables high peptide identification rates, individualized p.p.b.-range mass accuracies and proteome-wide protein quantification. *Nature Biotechnology*, 26(12), pp. 1367–1372. doi:10.1038/nbt.1511.

Freen-van Heeren, J.J., Popović, B., Guislain, A., Wolkers, M.C. and rich elements Human IFN-γ, Posttranscriptional regulation T cells (2020). Human T cells employ conserved AU-rich elements to fine-tune IFN-γ production. *Eur J Immunol*. 2020/03/18, 50(7), pp. 949–958. doi:10.1002/eji.201948458.

Gebauer, F., Schwarzl, T., Valcárcel, J. and Hentze, M.W. (2021). RNA-binding proteins in human genetic disease. *Nature reviews. Genetics*, 22(3), pp. 185–198. doi:10.1038/s41576-020-00302-y.

Gerstberger, S., Hafner, M., Ascano, M. and Tuschl, T. (2014). Evolutionary conservation and expression of human RNA-binding proteins and their role in human genetic disease. *Advances in experimental medicine and biology*, 825, pp. 1–55. doi:10.1007/978-1-4939-1221-6_1.

Gerstberger, S., Hafner, M. and Tuschl, T. (2014). A census of human RNA-binding proteins. *Nature Reviews Genetics*, 15(12), pp. 829–845. doi:10.1038/nrg3813.

Gomez-Eerland, R., Nuijen, B., Heemskerk, B., van Rooij, N., van den Berg, J.H., Beijnen, J.H., Uckert, W., Kvistborg, P., Schumacher, T.N., Haanen, J.B.A.G., *et al.* (2014). Manufacture of gene-modified human T-cells with a memory stem/central memory phenotype. *Human gene therapy methods*, 25(5), pp. 277–87. doi:10.1089/hgtb.2014.004.

Gonzalez-Perez, A.C., Stempel, M., Wyler, E., Urban, C., Piras, A., Hennig, T., Ganskih, S., Wei, Y., Heim, A., Landthaler, M., *et al.* (2021). The Zinc Finger Antiviral Protein ZAP Restricts Human Cytomegalovirus and Selectively Binds and Destabilizes Viral UL4/UL5 Transcripts. *mBio*, 12(3). doi:10.1128/mBio.02683-20.

Grammatikakis, I., Abdelmohsen, K. and Gorospe, M. (2017). Posttranslational control of HuR function. *Wiley interdisciplinary reviews. RNA*, 8(1). doi:10.1002/wrna.1372.

Han, Q., Bagheri, N., Bradshaw, E.M., Hafler, D.A., Lauffenburger, D.A. and Love, J.C. (2012). Polyfunctional responses by human T cells result from sequential release of cytokines. *Proceedings of the National Academy of Sciences*, 109(5), pp. 1607–1612. doi:10.1073/pnas.1117194109.

Hanieh, H., Masuda, K., Metwally, H., Chalise, J.P., Mohamed, M., Nyati, K.K., Standley, D.M., Li, S., Higa, M., Zaman, M.M., *et al.* (2018). Arid5a stabilizes OX40 mRNA in murine CD4+ T cells by recognizing a stem-loop structure in its 3'UTR. *European journal of immunology*, 48(4), pp. 593–604. doi:10.1002/eji.201747109.

Hodge, D.L., Berthet, C., Coppola, V., Kastenmüller, W., Buschman, M.D., Schaughency, P.M., Shirota, H., Scarzello, A.J., Subleski, J.J., Anver, M.R., *et al.* (2014). IFN-gamma AU-rich element removal promotes chronic IFN-gamma expression and autoimmunity in mice. *Journal of autoimmunity*, 53, pp. 33–45. doi:10.1016/j.jaut.2014.02.003.

Hodson, D.J., Janas, M.L., Galloway, A., Bell, S.E., Andrews, S., Li, C.M., Pannell, R., Siebel, C.W., MacDonald, H.R., De Keersmaecker, K., *et al.* (2010). Deletion of the RNA-binding proteins ZFP36L1 and ZFP36L2 leads to perturbed thymic development and T lymphoblastic leukemia. *Nature immunology*, 11(8), pp. 717–24. doi:10.1038/ni.1901.

Hoefig, K.P. and Heissmeyer, V. (2018). Posttranscriptional regulation of T helper cell fate decisions. *J Cell Biol*. 2018/04/23, 217(8), pp. 2615–2631. doi:10.1083/jcb.201708075.

Jurgens, A.P., Popović, B. and Wolkers, M.C. (2021). T cells at work: How post-transcriptional mechanisms control T cell homeostasis and activation. *European Journal of Immunology* [Preprint]. doi:10.1002/eji.202049055.

Kaehler, C., Isensee, J., Nonhoff, U., Terrey, M., Hucho, T., Lehrach, H. and Krobitsch, S. (2012). Ataxin-2-like is a regulator of stress granules and processing bodies. *PloS one*, 7(11), p. e50134. doi:10.1371/journal.pone.0050134.

Kim, H.H., Abdelmohsen, K., Lal, A., Pullmann, R., Yang, X., Galban, S., Srikantan, S., Martindale, J.L., Blethrow, J., Shokat, K.M., *et al.* (2008). Nuclear HuR accumulation through phosphorylation by Cdk1. *Genes & development*, 22(13), pp. 1804–15. doi:10.1101/gad.1645808.

König, J., Zarnack, K., Rot, G., Curk, T., Kayikci, M., Zupan, B., Turner, D.J., Luscombe, N.M. and Ule, J. (2010). iCLIP reveals the function of hnRNP particles in splicing at individual nucleotide resolution. *Nature structural & molecular biology*, 17(7), pp. 909–15. doi:10.1038/nsmb.1838.

Kontoyiannis, D., Pasparakis, M., Pizarro, T.T., Cominelli, F. and Kollias, G. (1999). Impaired on/off regulation of TNF biosynthesis in mice lacking TNF AU-rich elements: implications for joint and gut-associated immunopathologies. *Immunity*, 10(3), pp. 387–98. doi:10.1016/s1074-7613(00)80038-2.

Leppek, K. and Stoecklin, G. (2014). An optimized streptavidin-binding RNA aptamer for purification of ribonucleoprotein complexes identifies novel ARE-binding proteins. *Nucleic acids research*, 42(2), p. e13. doi:10.1093/nar/gkt956.

van der Leun, A.M., Thommen, D.S. and Schumacher, T.N. (2020). CD8 + T cell states in human cancer: insights from single-cell analysis. *Nat Rev Cancer*. 2020/02/05, 20(4), pp. 218–232. doi:10.1038/s41568-019-0235-4.

Lykke-Andersen, J. and Wagner, E. (2005). Recruitment and activation of mRNA decay enzymes by two ARE-mediated decay activation domains in the proteins TTP and BRF-1. *Genes & development*, 19(3), pp. 351–61. doi:10.1101/gad.1282305.

Marchese, F.P., Aubareda, A., Tudor, C., Saklatvala, J., Clark, A.R. and Dean, J.L.E. (2010). MAPKAP kinase 2 blocks tristetraprolin-directed mRNA decay by inhibiting CAF1 deadenylase recruitment. *The Journal of biological chemistry*, 285(36), pp. 27590–600. doi:10.1074/jbc.M110.136473.

Masuda, K., Ripley, B., Nyati, K.K., Dubey, P.K., Zaman, M.M.-U., Hanieh, H., Higa, M., Yamashita, K., Standley, D.M., Mashima, T., *et al.* (2016). Arid5a regulates naive CD4+ T cell fate through selective stabilization of Stat3 mRNA. *The Journal of experimental medicine*, 213(4), pp. 605–19. doi:10.1084/jem.20151289.

Mi, H., Muruganujan, A., Ebert, D., Huang, X. and Thomas, P.D. (2019). PANTHER version 14: more genomes, a new PANTHER GO-slim and improvements in enrichment analysis tools. *Nucleic Acids Research*, 47(D1), pp. D419–D426. doi:10.1093/nar/gky1038.

Moore, M.J., Blachere, N.E., Fak, J.J., Park, C.Y., Sawicka, K., Parveen, S., Zucker-Scharff, I., Moltedo, B., Rudensky, A.Y. and Darnell, R.B. (2018). ZFP36 RNA-binding proteins restrain T cell activation and anti-viral immunity. *eLife*, 7. doi:10.7554/eLife.33057.

Morita, S., Kojima, T. and Kitamura, T. (2000). Plat-E: an efficient and stable system for transient packaging of retroviruses. *Gene Therapy*, 7(12), pp. 1063–1066. doi:10.1038/sj.gt.3301206.

Nicolet, B.P., Guislain, A., van Alphen, F.P.J., Gomez-Eerland, R., Schumacher, T.N.M., van den Biggelaar, M. and Wolkers, M.C. (2020). CD29 identifies IFN-γ-producing human CD8+ T cells with an increased cytotoxic potential. *Proceedings of the National Academy of Sciences of the United States of America*, 117(12), pp. 6686–6696. doi:10.1073/pnas.1913940117.

Nicolet, B.P., Guislain, A. and Wolkers, M.C. (2017). Combined Single-Cell Measurement of Cytokine mRNA and Protein Identifies T Cells with Persistent Effector Function. *J Immunol*. 2016/12/07, 198(2), pp. 962–970. doi:10.4049/jimmunol.1601531.

Van Nostrand, E.L., Freese, P., Pratt, G.A., Wang, X., Wei, X., Xiao, R., Blue, S.M., Chen, J.-Y., Cody, N.A.L., Dominguez, D., *et al.* (2020). A large-scale binding and functional map of human RNA-binding proteins. *Nature*, 583(7818), pp. 711–719. doi:10.1038/s41586-020-2077-3.

Oh, D.Y., Kwek, S.S., Raju, S.S., Li, T., McCarthy, E., Chow, E., Aran, D., Ilano, A., Pai, C.-C.S., Rancan, C., *et al.* (2020). Intratumoral CD4+ T Cells Mediate Anti-tumor Cytotoxicity in Human Bladder Cancer. *Cell*, 181(7), pp. 1612-1625.e13. doi:10.1016/j.cell.2020.05.017.

Patel, S.J., Sanjana, N.E., Kishton, R.J., Eidizadeh, A., Vodnala, S.K., Cam, M., Gartner, J.J., Jia, L., Steinberg, S.M., Yamamoto, T.N., *et al.* (2017). Identification of essential genes for cancer immunotherapy. *Nature*, 548(7669), pp. 537–542. doi:10.1038/nature23477.

Perez-Perri, J.I., Rogell, B., Schwarzl, T., Stein, F., Zhou, Y., Rettel, M., Brosig, A. and Hentze, M.W. (2018). Discovery of RNA-binding proteins and characterization of their dynamic responses by enhanced RNA interactome capture. *Nature Communications*, 9(1), p. 4408. doi:10.1038/s41467-018-06557-8.

Philip, M. and Schietinger, A. (2021). CD8+ T cell differentiation and dysfunction in cancer. *Nature Reviews Immunology* [Preprint]. doi:10.1038/s41577-021-00574-3.

Quezada, S.A., Simpson, T.R., Peggs, K.S., Merghoub, T., Vider, J., Fan, X., Blasberg, R., Yagita, H., Muranski, P., Antony, P.A., *et al.* (2010). Tumor-reactive CD4+ T cells develop cytotoxic activity and eradicate large established melanoma after transfer into lymphopenic hosts. *Journal of Experimental Medicine*, 207(3), pp. 637–650. doi:10.1084/jem.20091918.

Raghavan, A., Robison, R.L., McNabb, J., Miller, C.R., Williams, D.A. and Bohjanen,

P.R. (2001). HuA and tristetraprolin are induced following T cell activation and display distinct but overlapping RNA binding specificities. *The Journal of biological chemistry*, 276(51), pp. 47958–65. doi:10.1074/jbc.M109511200.

Salerno, F., Engels, S., van den Biggelaar, M., van Alphen, F.P.J., Guislain, A., Zhao, W., Hodge, D.L., Bell, S.E., Medema, J.P., von Lindern, M., *et al.* (2018). Translational repression of pre-formed cytokine-encoding mRNA prevents chronic activation of memory T cells. *Nature Immunology*, 19(8), pp. 828–837. doi:10.1038/s41590-018-0155-6.

Salerno, F., Freen-van Heeren, J.J., Guislain, A., Nicolet, B.P. and Wolkers, M.C. (2019). Costimulation through TLR2 Drives Polyfunctional CD8 + T Cell Responses. *The Journal of Immunology*, 202(3), pp. 714–723. doi:10.4049/jimmunol.1801026.

Salerno, F., Guislain, A., Cansever, D. and Wolkers, M.C. (2016). TLR-Mediated Innate Production of IFN-γ by CD8 + T Cells Is Independent of Glycolysis. *The Journal of Immunology*, 196(9), pp. 3695–3705. doi:10.4049/jimmunol.1501997.

Salerno, F., Guislain, A., Freen-Van Heeren, J.J., Nicolet, B.P., Young, H.A. and Wolkers, M.C. (2019). Critical role of post-transcriptional regulation for IFN-γ in tumor-infiltrating T cells. *OncoImmunology*, 8(2). p. e1532762. doi:10.1080/2162402X.2018.1532762.

Salerno, F., Paolini, N.A., Stark, R., von Lindern, M. and Wolkers, M.C. (2017). Distinct PKC-mediated posttranscriptional events set cytokine production kinetics in CD8(+) T cells. *Proc Natl Acad Sci U S A*. 2017/08/23, 114(36), pp. 9677–9682. doi:10.1073/pnas.1704227114.

Salerno, F., Turner, M. and Wolkers, M.C. (2020). Dynamic Post-Transcriptional Events Governing CD8+ T Cell Homeostasis and Effector Function. *Trends in Immunology*, 41(3). pp. 240-254. doi:10.1016/j.it.2020.01.001.

Sandler, H., Kreth, J., Timmers, H.T.M. and Stoecklin, G. (2011). Not1 mediates recruitment of the deadenylase Caf1 to mRNAs targeted for degradation by tristetraprolin. *Nucleic acids research*, 39(10), pp. 4373–86. doi:10.1093/nar/gkr011.

Schwerk, J., Soveg, F.W., Ryan, A.P., Thomas, K.R., Hatfield, L.D., Ozarkar, S., Forero, A., Kell, A.M., Roby, J.A., So, L., *et al.* (2019). RNA-binding protein isoforms ZAP-S and ZAP-L have distinct antiviral and immune resolution functions. *Nature Immunology*, 20(12), pp. 1610–1620. doi:10.1038/s41590-019-0527-6.

Srikantan, S., Tominaga, K. and Gorospe, M. (2012). Functional interplay between RNA-binding protein HuR and microRNAs. *Current protein & peptide science*, 13(4), pp. 372–9. doi:10.2174/138920312801619394.

van Stipdonk, M.J., Hardenberg, G., Bijker, M.S., Lemmens, E.E., Droin, N.M., Green, D.R. and Schoenberger, S.P. (2003). Dynamic programming of CD8+ T lymphocyte responses. *Nat Immunol*. 2003/03/17, 4(4), pp. 361–365. doi:10.1038/ni912.

Tiedje, C., Ronkina, N., Tehrani, M., Dhamija, S., Laass, K., Holtmann, H., Kotlyarov, A. and Gaestel, M. (2012). The p38/MK2-driven exchange between tristetraprolin and HuR regulates AU-rich element-dependent translation. *PLoS genetics*, 8(9), p. e1002977. doi:10.1371/journal.pgen.1002977.

Vogel, K.U., Bell, L.S., Galloway, A., Ahlfors, H. and Turner, M. (2016). The RNA-Binding Proteins Zfp36l1 and Zfp36l2 Enforce the Thymic β-Selection Checkpoint by Limiting DNA Damage Response Signaling and Cell Cycle Progression. *Journal of immunology (Baltimore, Md.□: 1950)*, 197(7), pp. 2673–2685. doi:10.4049/jimmunol.1600854.

Wimmers, F., Aarntzen, E.H.J.G., Duiveman-deBoer, T., Figdor, C.G., Jacobs, J.F.M., Tel, J. and de Vries, I.J.M. (2016). Long-lasting multifunctional CD8+ T cell responses in end-stage melanoma patients can be induced by dendritic cell vaccination. *OncoImmunology*, 5(1), p. e1067745. doi:10.1080/2162402X.2015.1067745.

de Witte, M.A., Coccoris, M., Wolkers, M.C., van den Boom, M.D., Mesman, E.M., Song, J.-Y., van der Valk, M., Haanen, J.B.A.G. and Schumacher, T.N.M. (2006). Targeting self-antigens through allogeneic TCR gene transfer. *Blood*, 108(3), pp. 870–7. doi:10.1182/blood-2005-08-009357.

Yoon, J.-H., Abdelmohsen, K., Srikantan, S., Guo, R., Yang, X., Martindale, J.L. and Gorospe, M. (2014). Tyrosine phosphorylation of HuR by JAK3 triggers dissociation and degradation of HuR target mRNAs. *Nucleic acids research*, 42(2), pp. 1196–208. doi:10.1093/nar/gkt903.

Yoshinaga, M. and Takeuchi, O. (2019). Post-transcriptional control of immune responses and its potential application. *Clinical & Translational Immunology*, 8(6). p. e1063. doi:10.1002/cti2.1063.

Zandhuis, N.D., Nicolet, B.P. and Wolkers, M.C. (2021). Mapping RNA-binding proteins in human B cells and T cells upon differentiation. *bioRxiv* [Preprint]. doi:10.1101/2021.06.10.447413.

Zhang, B., Karrison, T., Rowley, D.A. and Schreiber, H. (2008). IFN-gamma- and TNF-dependent bystander eradication of antigen-loss variants in established mouse cancers. *The Journal of clinical investigation*, 118(4), pp. 1398–404. doi:10.1172/JCI33522.

Zhang, X., Smits, A.H., van Tilburg, G.B., Ovaa, H., Huber, W. and Vermeulen, M. (2018). Proteome-wide identification of ubiquitin interactions using UbIA-MS. *Nature Protocols*, 13(3), pp. 530–550. doi:10.1038/nprot.2017.147.

Zimmer, M.M., Kibe, A., Rand, U., Pekarek, L., Cicin-Sain, L. and Caliskan, N. (2021). Revealing the host antiviral protein ZAP-S as an inhibitor of SARS-CoV-2 programmed ribosomal frameshifting. *biorxiv* [Preprint]. doi:10.1101/2021.05.31.445667.

Figure 1

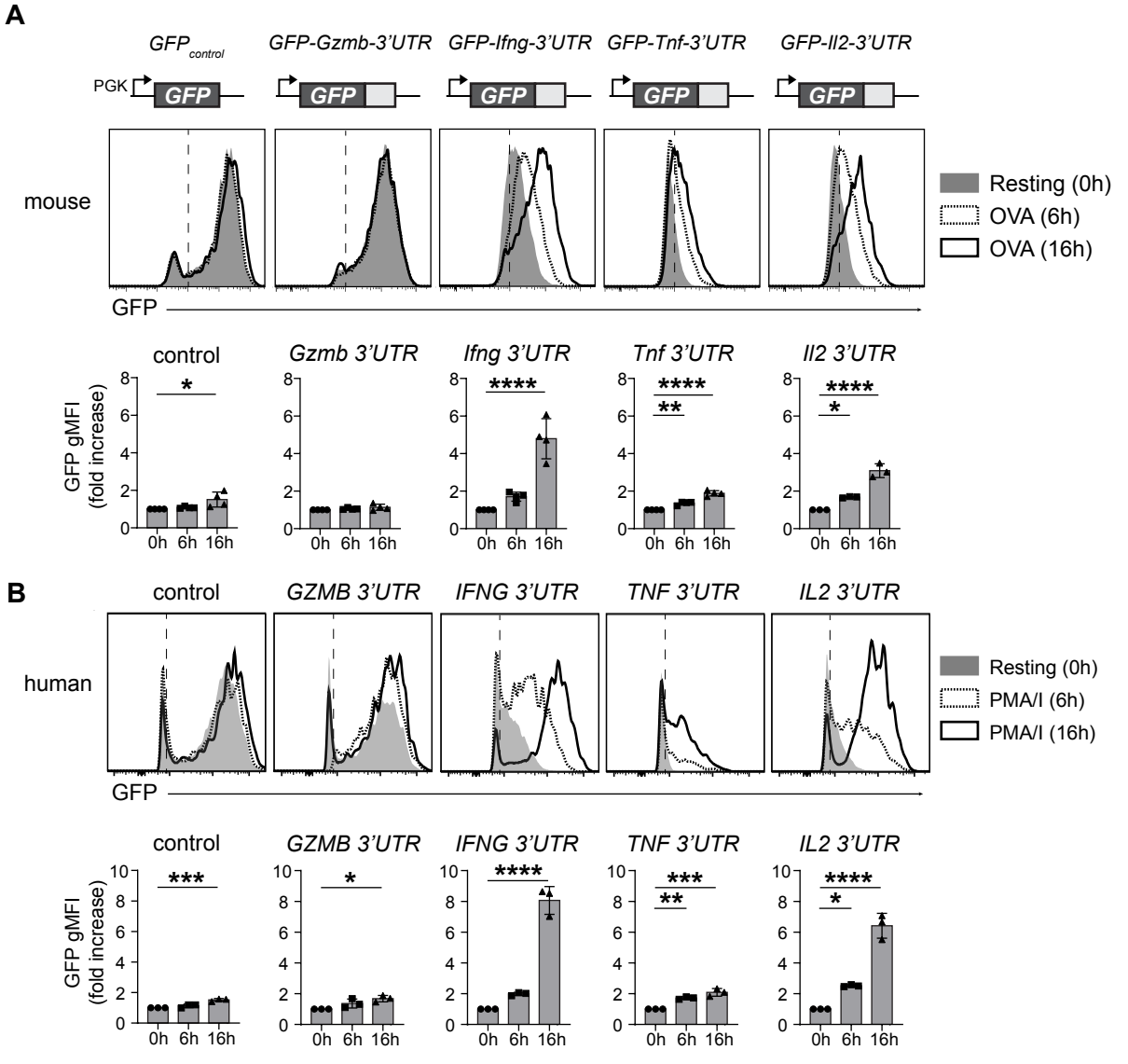
A
GFP control
GFP-Gzmb-3'UTR
GFP-Ifng-3'UTR
GFP-Tnf-3'UTR
GFP-Il2-3'UTR
PGK
GFP
mouse
Resting (0h)
OVA (6h)
OVA (16h)
GFP
control
Gzmb 3'UTR
Ifng 3'UTR
Tnf 3'UTR
Il2 3'UTR
GFP gMFI (fold increase)
0h 6h 16h
B
control
GZMB 3'UTR
IFNG 3'UTR
TNF 3'UTR
IL2 3'UTR
human
Resting (0h)
PMA/I (6h)
PMA/I (16h)
GFP
GFP gMFI (fold increase)
0h 6h 16h

Figure 2

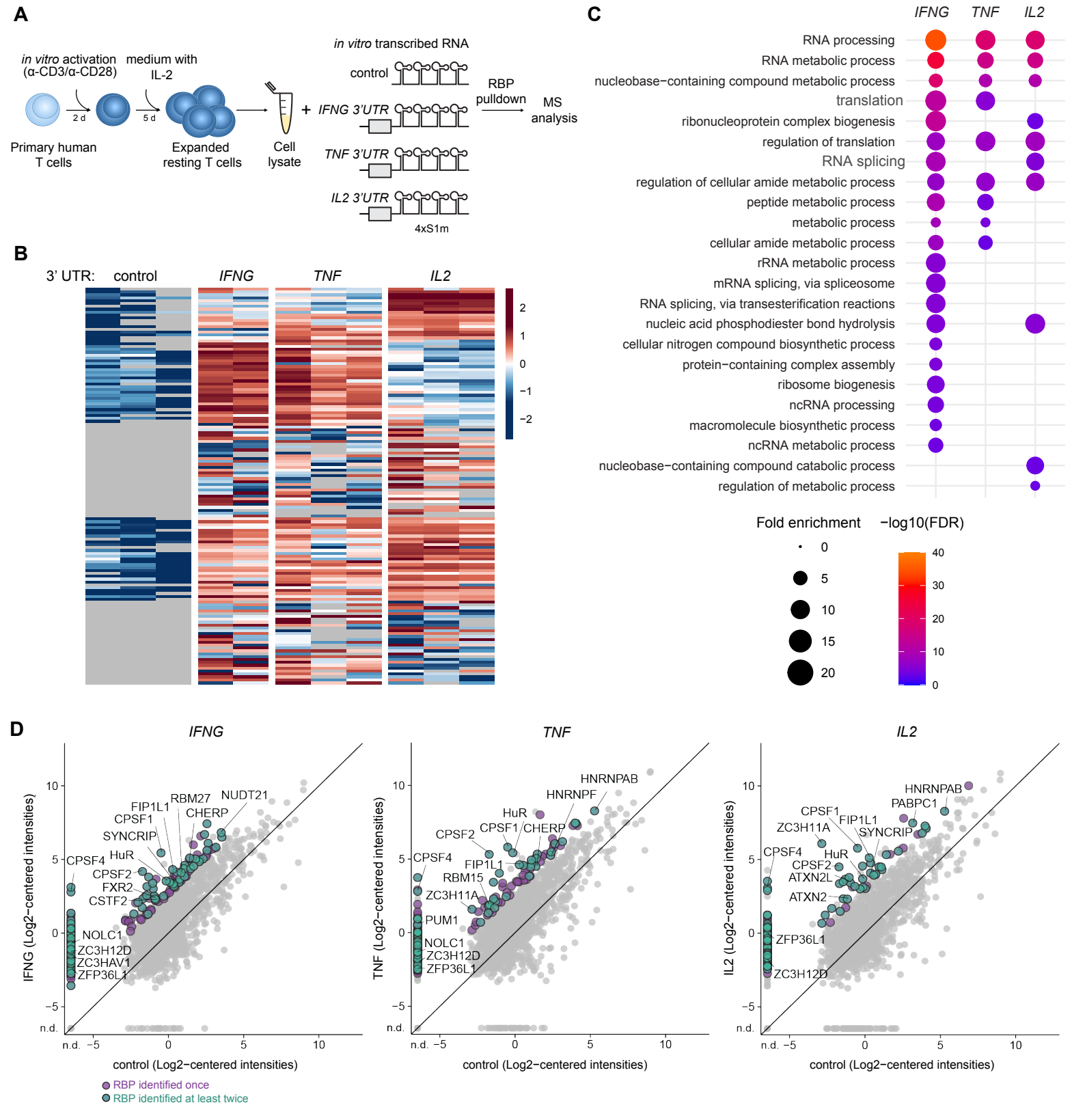
A
in vitro activation (α-CD3/α-CD28)
medium with IL-2
2 d
5 d
Primary human T cells
Expanded resting T cells
Cell lysate
in vitro transcribed RNA
control
IFNG 3'UTR
TNF 3'UTR
IL2 3'UTR
4xS1m
RBP pulldown
MS analysis
B
3' UTR: control
IFNG
TNF
IL2
C
IFNG
TNF
IL2
RNA processing
RNA metabolic process
nucleobase−containing compound metabolic process
translation
ribonucleoprotein complex biogenesis
regulation of translation
RNA splicing
regulation of cellular amide metabolic process
peptide metabolic process
metabolic process
cellular amide metabolic process
rRNA metabolic process
mRNA splicing, via spliceosome
RNA splicing, via transesterification reactions
nucleic acid phosphodiester bond hydrolysis
cellular nitrogen compound biosynthetic process
protein−containing complex assembly
ribosome biogenesis
ncRNA processing
macromolecule biosynthetic process
ncRNA metabolic process
nucleobase−containing compound catabolic process
regulation of metabolic process
Fold enrichment
−log10(FDR)
D
IFNG
TNF
IL2
IFNG (Log2−centered intensities)
TNF (Log2−centered intensities)
IL2 (Log2−centered intensities)
control (Log2−centered intensities)
n.d.
NUDT21
RBM27
FIP1L1
CPSF1
CHERP
SYNCRIP
HuR
CPSF4
CPSF2
FXR2
CSTF2
NOLC1
ZC3H12D
ZC3HAV1
ZFP36L1
HNRNPAB
HNRNPF
CPSF2
RBM15
ZC3H11A
PUM1
PABPC1
ZC3H11A
ATXN2L
ATXN2
RBP identified once
RBP identified at least twice

Figure 3

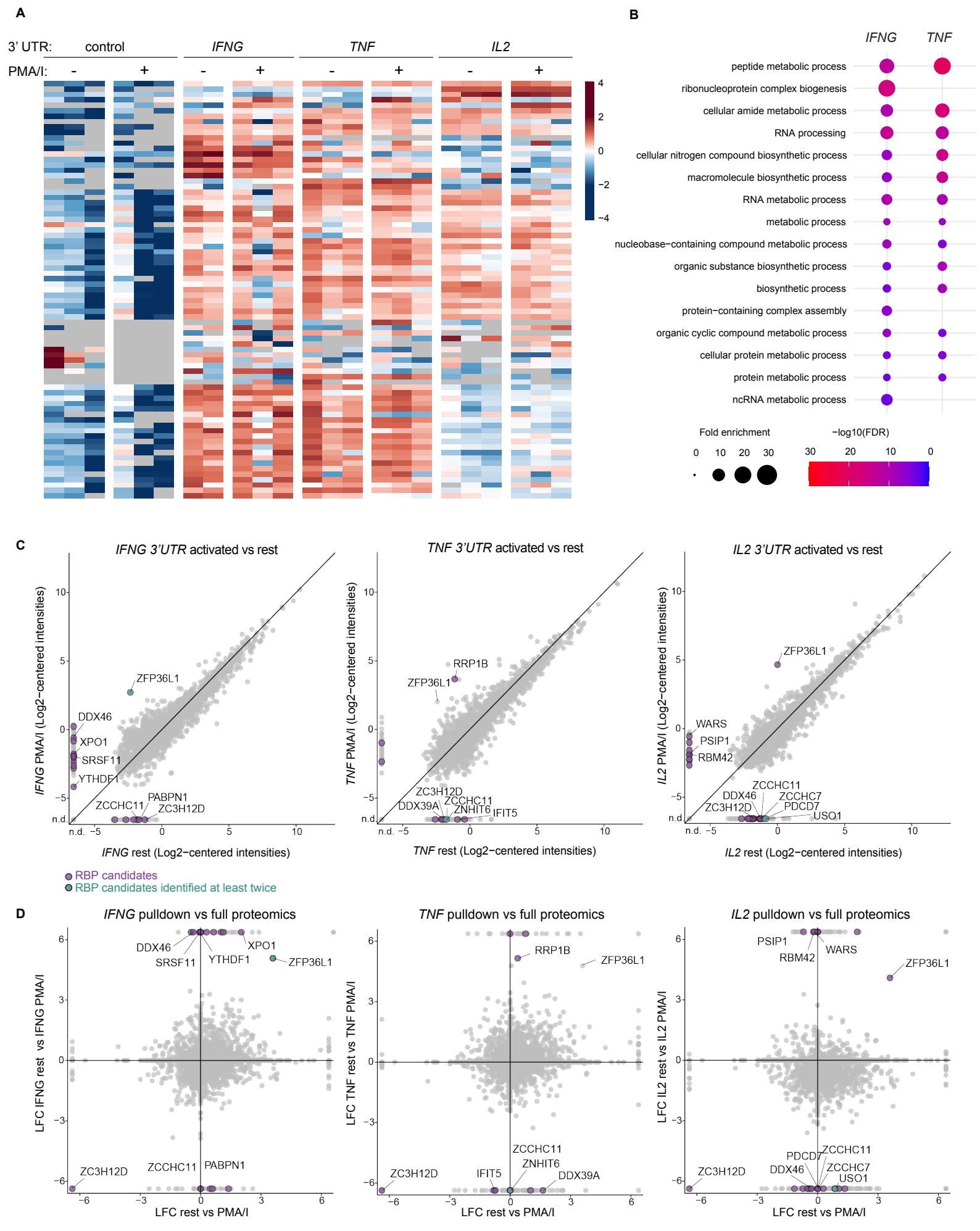
A
3' UTR: control IFNG TNF IL2
PMA/I: - + - + - + - +
4
2
0
−2
−4
B
IFNG TNF
peptide metabolic process
ribonucleoprotein complex biogenesis
cellular amide metabolic process
RNA processing
cellular nitrogen compound biosynthetic process
macromolecule biosynthetic process
RNA metabolic process
metabolic process
nucleobase−containing compound metabolic process
organic substance biosynthetic process
biosynthetic process
protein−containing complex assembly
organic cyclic compound metabolic process
cellular protein metabolic process
protein metabolic process
ncRNA metabolic process
Fold enrichment
0 10 20 30
−log10(FDR)
30 20 10 0
C
IFNG 3'UTR activated vs rest
IFNG PMA/I (Log2−centered intensities)
IFNG rest (Log2−centered intensities)
ZFP36L1
DDX46
XPO1
SRSF11
YTHDF1
PABPN1
ZCCHC11
ZC3H12D
TNF 3'UTR activated vs rest
TNF PMA/I (Log2−centered intensities)
TNF rest (Log2−centered intensities)
RRP1B
ZFP36L1
ZC3H12D
DDX39A
ZCCHC11
ZNHIT6
IFIT5
IL2 3'UTR activated vs rest
IL2 PMA/I (Log2−centered intensities)
IL2 rest (Log2−centered intensities)
ZFP36L1
WARS
PSIP1
RBM42
ZCCHC11
DDX46
ZCCHC7
ZC3H12D
PDCD7
USO1
n.d.
RBP candidates
RBP candidates identified at least twice
D
IFNG pulldown vs full proteomics
LFC IFNG rest vs IFNG PMA/I
LFC rest vs PMA/I
DDX46
SRSF11
YTHDF1
XPO1
ZFP36L1
ZC3H12D
ZCCHC11
PABPN1
TNF pulldown vs full proteomics
LFC TNF rest vs TNF PMA/I
LFC rest vs PMA/I
RRP1B
ZFP36L1
ZCCHC11
ZNHIT6
ZC3H12D
IFIT5
DDX39A
IL2 pulldown vs full proteomics
LFC IL2 rest vs IL2 PMA/I
LFC rest vs PMA/I
PSIP1
RBM42
WARS
ZFP36L1
PDCD7
ZCCHC11
ZC3H12D
DDX46
ZCCHC7
USO1

Figure 4

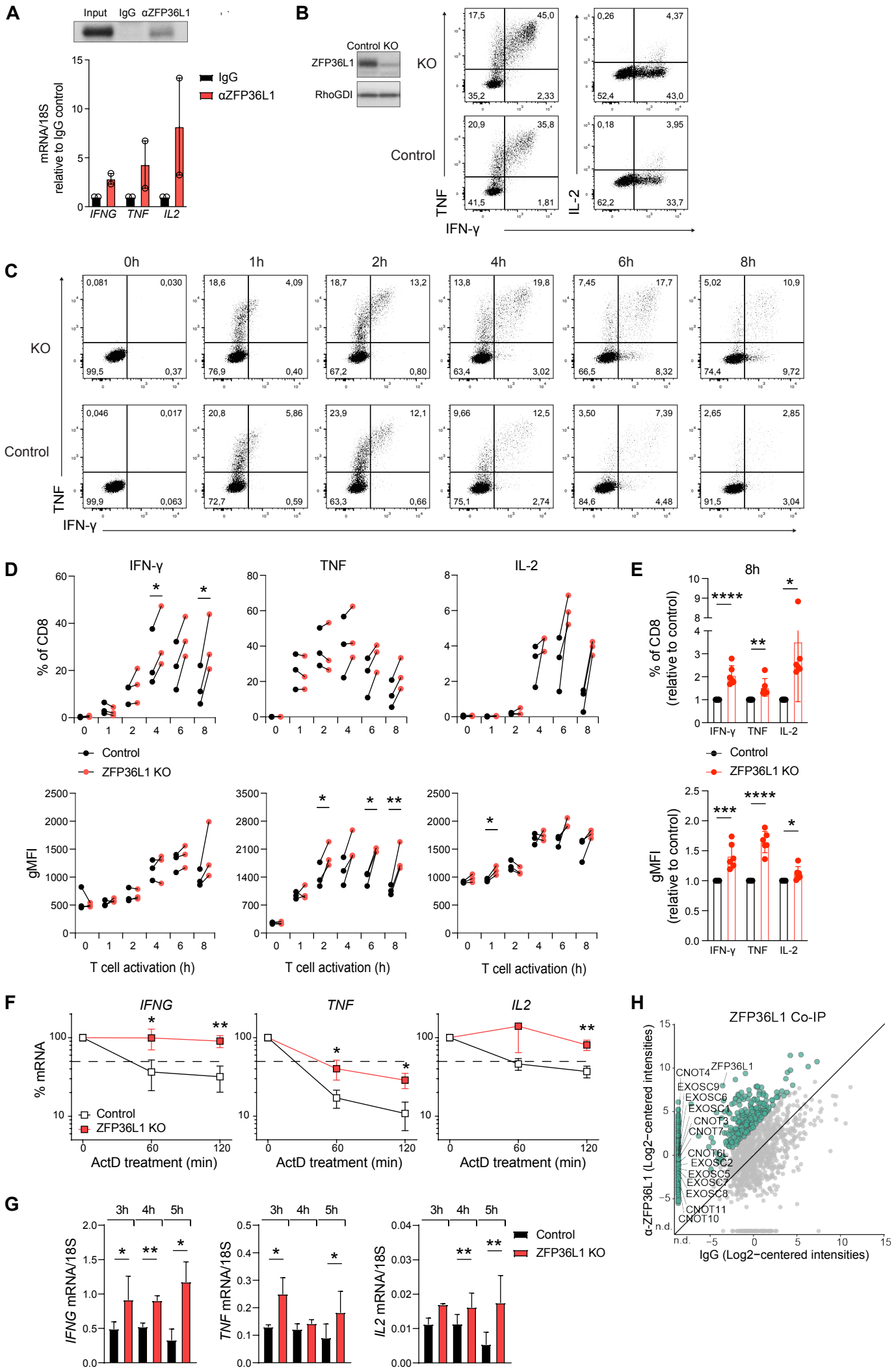
A
Input IgG αZFP36L1
mRNA/18S relative to IgG control
IgG
αZFP36L1
IFNG TNF IL2
B
Control KO
ZFP36L1
RhoGDI
KO
Control
TNF
IFN-γ
IL-2
C
0h 1h 2h 4h 6h 8h
KO
Control
TNF
IFN-γ
D
IFN-γ
TNF
IL-2
% of CD8
Control
ZFP36L1 KO
gMFI
T cell activation (h)
E
8h
% of CD8 (relative to control)
IFN-γ TNF IL-2
gMFI (relative to control)
F
IFNG
TNF
IL2
% mRNA
ActD treatment (min)
G
3h 4h 5h
IFNG mRNA/18S
TNF mRNA/18S
IL2 mRNA/18S
H
ZFP36L1 Co-IP
α-ZFP36L1 (Log2−centered intensities)
IgG (Log2−centered intensities)
CNOT4
ZFP36L1
EXOSC9
EXOSC6
EXOSC1
CNOT3
CNOT7
CNOT6L
EXOSC2
EXOSC5
EXOSC7
EXOSC8
CNOT11
CNOT10
n.d.

Figure 5

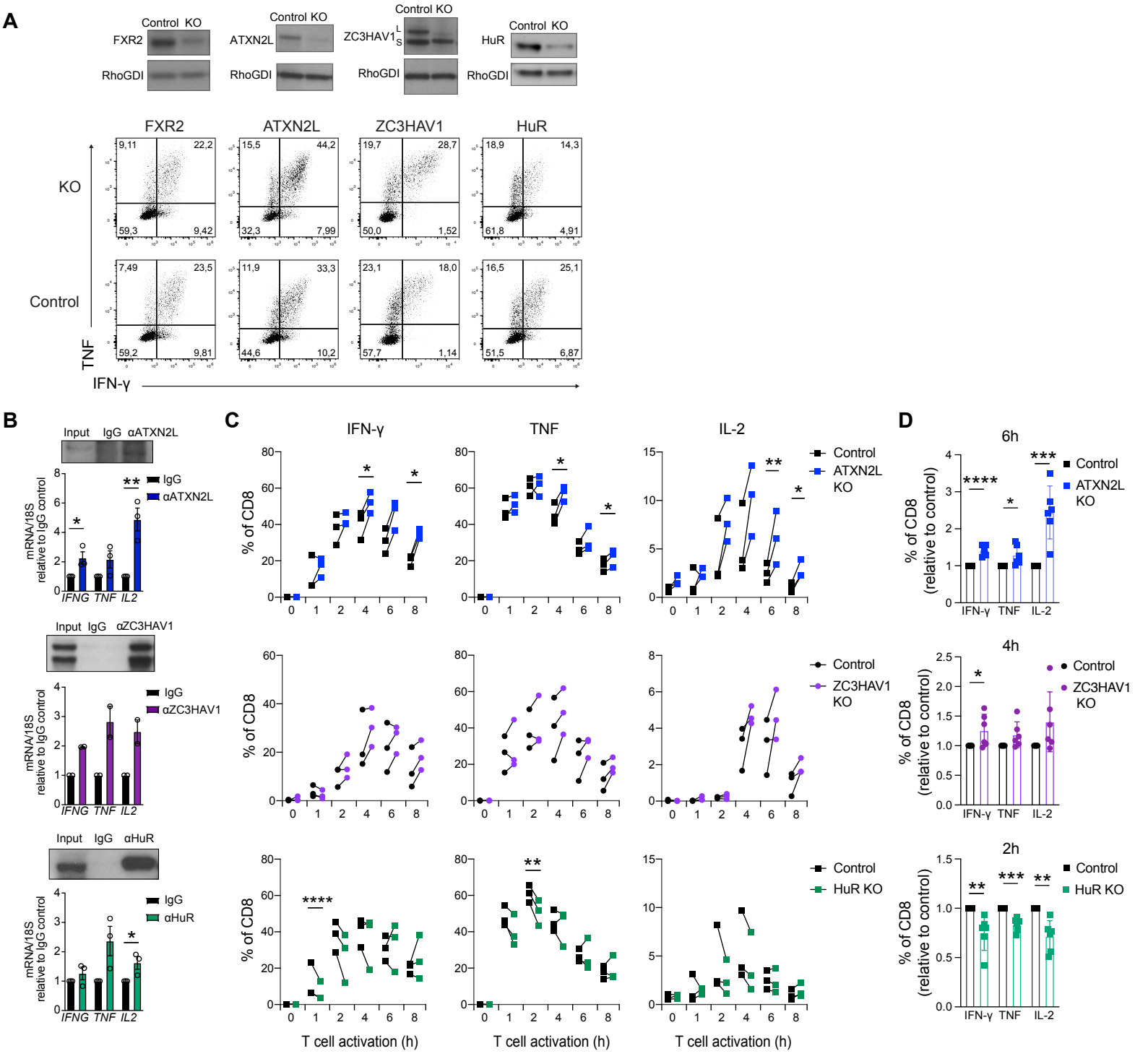
A
Control KO
FXR2
RhoGDI
ATXN2L
ZC3HAV1
HuR
FXR2
ATXN2L
ZC3HAV1
HuR
KO
Control
TNF
IFN-γ
B
Input IgG αATXN2L
IgG
αATXN2L
mRNA/18S relative to IgG control
IFNG TNF IL2
Input IgG αZC3HAV1
αZC3HAV1
Input IgG αHuR
αHuR
C
IFN-γ
TNF
IL-2
% of CD8
Control
ATXN2L KO
ZC3HAV1 KO
HuR KO
T cell activation (h)
D
6h
4h
2h
% of CD8 (relative to control)
IFN-γ TNF IL-2

Figure 6

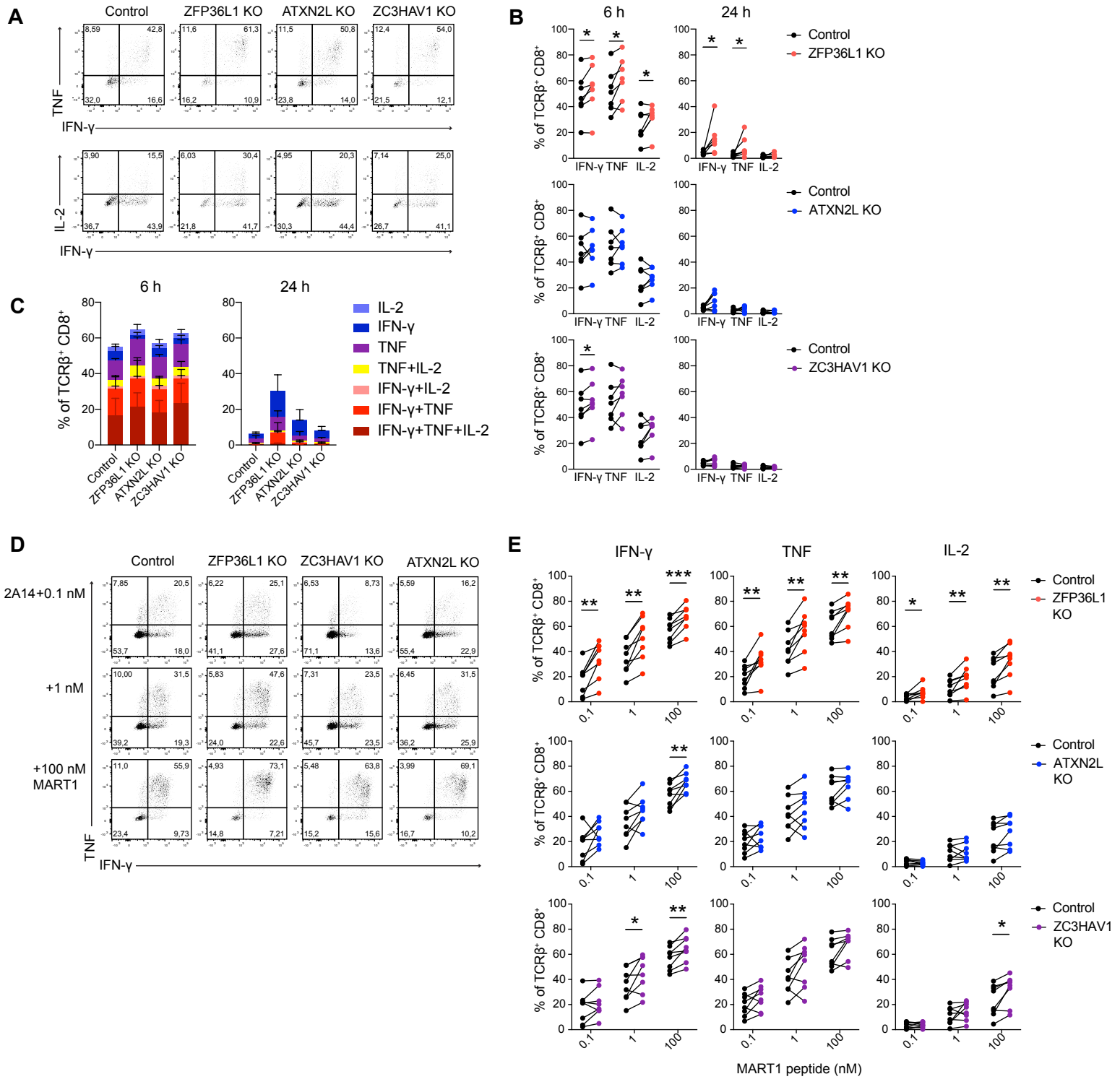
A
Control
ZFP36L1 KO
ATXN2L KO
ZC3HAV1 KO
TNF
IFN-γ
IL-2
B
6 h
24 h
% of TCRβ+ CD8+
IFN-γ TNF IL-2
Control
ZFP36L1 KO
ATXN2L KO
ZC3HAV1 KO
C
IL-2
IFN-γ
TNF
TNF+IL-2
IFN-γ+IL-2
IFN-γ+TNF
IFN-γ+TNF+IL-2
D
2A14+0.1 nM
+1 nM
+100 nM MART1
E
IFN-γ
TNF
IL-2
MART1 peptide (nM)

Figure 7

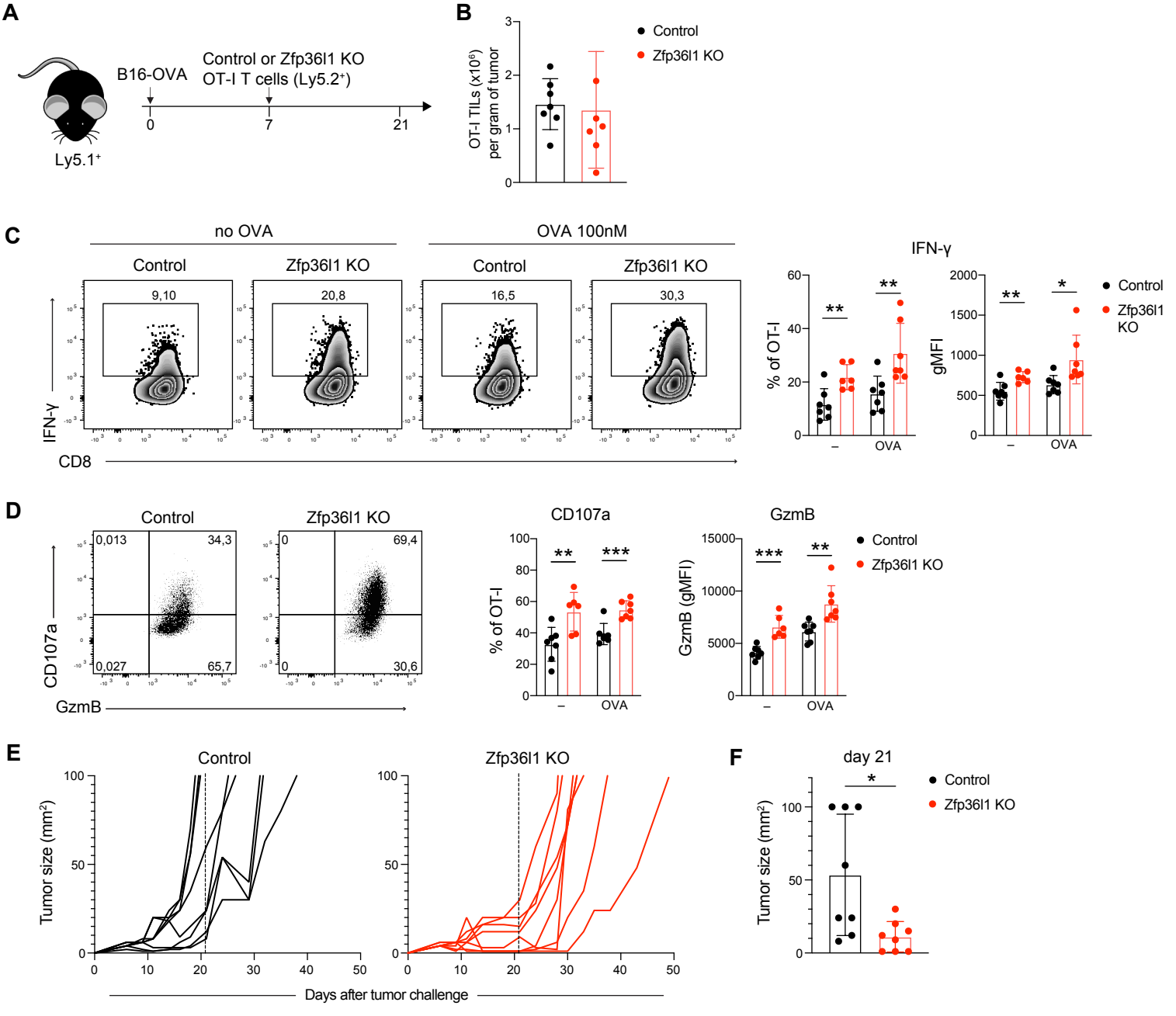
A
B16-OVA
Control or Zfp36l1 KO
OT-I T cells (Ly5.2⁺)
0
7
21
Ly5.1⁺
B
OT-I TILs (x10⁶) per gram of tumor
Control
Zfp36l1 KO
C
no OVA
OVA 100nM
Control
Zfp36l1 KO
9,10
20,8
16,5
30,3
IFN-γ
CD8
% of OT-I
gMFI
OVA
D
0,013
34,3
0,027
65,7
0
69,4
30,6
CD107a
GzmB
GzmB (gMFI)
E
Tumor size (mm²)
Days after tumor challenge
F
day 21